Responses to Reviewer 2
I have to stress that my recommendation is NOT based on the satisfactory revisions (the revisions are relatively minor), but because of my expectation that the peer review process has to stop at some point. I strongly feel that the authors' interpretation of the invigoration problem is biased and this affects the discussion of past studies and current model results. For instance, on lines 52/53 the authors say that Grabowski and Morrison (2016, 2020) "reject […] invigoration concept". This is not true: Grabowski and Morrison argue that the simplistic view of the invigoration is difficult to understand based on the buoyancy below and above the freezing level in situation without and with pollution. On lines 81/84, the authors refer to Varble (2018) arguing that Varble's study suggests that 10 years of SGP data is not sufficient to separate meteorological factors from the impact of aerosol. This is not true: Varble shows that meteorological conditions over SGP explain observed changes in convection without referring to aerosols, and that the 10-year study the authors implicitly refer to is severely flawed. It is impossible for me to point all places where the authors are biased. I thus suggest that the paper is published, perhaps with some final changes following my comments below. That said, I have to stress – as I did before – that the manuscript does not need to refer to the invigoration. The difference between saturation-adjustment in the Morrison bulk scheme and saturation-prediction in the Khain bin scheme is sufficient to explain the differences. The strength of the manuscript is in a direct prediction of CCN formation and removal, and how these can be linked to cloud processes.

We are glad that the reviewer now softened their arguments in Grabowski and Morrison (2016, 2020). Here are the original sentences from the abstract and conclusion of those two papers:
"There is no impact on convective dynamics above the freezing level and thus no convective invigoration" (abstract of GM16); "In summary, the invigoration of deep convection in polluted environments, either resulting from increased total CCN concentrations as suggested in Rosenfeld et al. (2008) or from addition of small CCN to the pristine environment as in Fan et al. (2018), is not supported by theoretical arguments and cloud simulations presented here" (Conclusion of GM20).
So our statement is the exact message that the authored delivered in their papers. Anyway we reworded the sentences at Line 51-52: "Grabowski and Morrison (2016; 2020) argued this invigoration does not exist because the increase in the buoyancy by freezing is completely offset by the buoyancy for carrying the extra cloud water across the freezing level."
About Varble (2018), the paper clearly stated "It will be shown that for the Atmospheric Radiation Measurement (ARM) Southern Great Plains (SGP) site in north-central Oklahoma, 14 years of observations are not sufficient for concluding that increased aerosol concentrations cause an increase in cloud-top height and decrease in CTT…".
We would like to point out to the reviewer that Varble 2018 used the CAPE from the convective storm period, not the pre-convection environment CAPE. That was a problem for the analysis since the CAPE from convective period already accounted for the microphysics feedback to dynamics. Even with that, the study did not rebut the invigoration. It stated clearly "These results do not draw into question the validity of the well-reasoned aerosol convective invigoration hypothesis for certain environmental conditions. Rather, they highlight the need for more careful, detailed, and strategic observational analyses…".

The only more important and still unanswered point made in a couple of my previous comments is that the differences in the representation of ice processes in the two schemes, and how they are linked to warm-rain process, need to be clearly explained. For instance, is the ice initiation the same in both schemes? A short paragraph for each scheme should be sufficient.

As explained in the previous responses, SBM and Morrison are completely two different realizations of cloud microphysics so they are different in the way of treating every microphysical processes. Since our results showed that the main reason responsible for the different aerosol effect on the convective storm is the treatment of condensation and evaporation, we do not think laying out all the other model differences are important and it would take long text which would distract the paper. But, we added a couple of sentences to mention the differences in ice processes:
"The SBM and Morrison schemes are two completely different representations of cloud microphysics so they are different in many aspects including major microphysical processes such as aerosol activation, condensation/evaporation, collisions, and ice nucleation and ice growth through riming and aggregation. Details are read from Khain et al. (2004; 2015), Morrsion et al. (2015) and Gao et al. (2016)".

Another general comment is that English needs some improvements throughout the text. Some places are listed below.
We did a careful review to improve the language now. For the specific comments below, see our response one-by-one.

Specific comments:
1. The last sentence of the abstract is unclear. First, saturation adjustment provides the maximum buoyancy, so I do not understand why "saturation adjustment […] limits the enhancement in condensation…". I would think the opposite should be true. The (2) seemingly refers to ice processes, but it is unclear why saturation adjustment affects conversion of droplets into raindrops, and how these are related to ice processes.

Here what we said is that the saturation adjustment limited the aerosol effect, which does not conflict with saturation adjustment provides the maximum buoyancy. The saturation adjustment limits the enhancement in condensation latent heat from clean to polluted conditions because it removes the dependence of condensation on droplets/aerosols.
About why saturation adjustment affects conversion of droplets into raindrops and how these are related to ice processes, the reviewer missed the part of the analysis of this study, which is detailed at Line 410-433. In short, the saturation adjustment leads to larger droplet sizes in the warm cloud stage than the explicit supersaturation (i.e., MOR_anth vs MOR_SS_anth), leading to more efficient conversion of droplets into raindrops, which leaves less droplets available for being transported to the altitudes above the freezing level at the mixed-phase and deep cloud stages, thus weaker ice microphysical processes are seen. We have reworded the sentence to make it easier to understand, "…mainly because the saturation adjustment approach for droplet condensation and evaporation calculation limits the enhancement by aerosols in (1) condensation latent heat by removing the dependence of condensation on droplets/aerosols and (2) ice-related processes

because the approach leads to stronger warm rain and weaker ice processes than the explicit supersaturation approach".

2. L. 195. "The meteorological fields were reinitialized…"

Changed.

3. L. 225/227. The sentence: "…the supersaturation is solved by the source and sink in terms of dynamic forcing and condensation/evaporation within a one-timestep" needs to be rewritten. I commented on the subsequent sentence in the previous round ("…the supersaturation for condensation and evaporation is calculated after the advection."), see my point 2 in the previous review. Please revise.

Modified as suggested: "That is, the supersaturation is solved semi-analytically based on both the forcing from advection and the microphysics processes."

4. L. 252 should be "Results".

Changed.

5. Discussion of Figs. 7 an 8. I am not sure if I see differences between left and right panels in Fig.7. These are just different convection realizations to me. Can one apply an objective analysis to prove that? In Fig. 8, it is difficult for me to see which model simulation is closer to the observation with the exception of the echo top, higher in bin microphysics and in agreement with the radar plot.

The objective analysis/description was already shown in Line 310-324. In Fig.7, SBM_anth simulates the storm closer to the observation in both location and high reflectivity value (greater than 55 dBZ) than MOR_anth. In Fig.8, SBM_anth is in a better agreement with observation in terms of vertical structure of the high reflectivity range (> 48 dBZ) and echo top heights. MOR_anth did not simulate any occurrence of reflectivity larger than 55 dBZ.

6. Fig. 9. The authors ignored my suggestion to plot rain accumulation as more meaningful and less dependent on the specific realization of the flow.

As responded previously, we described the rain accumulation with text (Line 322-324; Line 338-340) since no figure is necessary for such a quantity given we have so many figures already.

7. Section 4.2, lines 405-456, the interpretation of results related to the impact of pollution on the supersaturation and particle growth between the two microphysics schemes. As I stated previously (and above), a brief description of ice microphysics between the two schemes, and the key differences, would provide a proper context for this discussion.

As also clarified in our previous response, the discussion for this part is based on the results from MOR and MOR_SS. There is no difference in ice microphysics between them and the test is only for the effect of different treatment of condensation/evaporation.

8. L. 481: "condenses all supersaturation". Perhaps "removes"?

"Condenses" is changed to "removes".

1 **Impacts of Cloud Microphysics Parameterizations on Simulated Aerosol-Cloud-Interactions**

2 **for Deep Convective Clouds over Houston**

3

4 Yuwei Zhang[1, 2], Jiwen Fan[2, *], Zhanqing Li[1], Daniel Rosenfeld[3]

5

6 [1]Department of Atmospheric and Oceanic Science, University of Maryland, College Park, MD,

7 USA

8 [2]Atmospheric Sciences and Global Change Division, Pacific Northwest National Laboratory,

9 Richland, WA, USA

10 [3] Institute of Earth Sciences, The Hebrew University of Jerusalem, Jerusalem, Israel

11 * *Correspondence to*: Jiwen Fan (jiwen.fan@pnnl.gov)

12

13

Abstract

Aerosol-cloud interactions remain largely uncertain in predicting their impacts on weather and climate. Cloud microphysics parameterization is one of the factors leading to large uncertainty. Here we investigate the impacts of anthropogenic aerosols on the convective intensity and precipitation of a thunderstorm occurring on 19 June 2013 over Houston with the Chemistry version of Weather Research and Forecast model (WRF-Chem) using the Morrison two-moment bulk scheme and spectral-bin microphysics (SBM) scheme. We find that the SBM predicts a deep convective cloud agreeing better with observations in terms of reflectivity and precipitation compared with the Morrison bulk scheme that has been used in many weather and climate models. With the SBM scheme, we see a significant invigoration effect on convective intensity and precipitation by anthropogenic aerosols mainly through enhanced condensation latent heating. Whereas such an effect is absent with the Morrison two-moment bulk microphysics, mainly because the saturation adjustment approach for droplet condensation and evaporation calculation limits the enhancement by aerosols in (1) condensation latent heat by removing the dependence of condensation on droplets/aerosols and (2) ice-related processes because the approach leads to stronger warm rain and weaker ice processes than the explicit supersaturation approach.

1 Introduction

Deep convective clouds (DCCs) produce copious precipitation and play important roles in the hydrological and energy cycle as well as regional and global circulation (e.g., Arakawa, 2004; Houze, 2014). DCCs and associated precipitation are determined by water vapor, vertical motion of air, and cloud microphysics that could be affected by aerosols through aerosol-radiative interactions (ARI) or aerosol-cloud interactions (ACI) or both. The cloud-mediated aerosol effects are recognized by the Intergovernmental Panel on Climate Change (IPCC) as one of the key sources of uncertainty in our knowledge of Earth's energy budget and anthropogenic climate forcing (e.g., Arakawa, 2004; Andreae et al., 2005; Haywood and Boucher, 2000; Lohmann and Feichter, 2005).

Precipitation, latent heat, and cloud radiative forcing associated with DCCs are strongly associated with cloud microphysical processes, which can be modulated by aerosols through serving as cloud condensation nuclei (CCN) and ice nuclei (IN). For aerosol-DCC interactions, a well-known theory is that increasing aerosol concentrations can suppress warm rain as a result of increased droplet numbers but reduced droplet size. This allows more cloud droplets to be lifted to altitudes above the freezing level, inducing stronger ice microphysical processes (e.g., droplet freezing, riming, and deposition) which release larger latent heating, thereby invigorating convective updrafts (referred to as "cold-phase invigoration,"; Khain et al. 2005; Rosenfeld et al., 2008). It is significant in the situations of warm-cloud bases (> 15°C; Fan et al., 2012b; Li et al., 2011; Rosenfeld et al., 2014; Tao and Li, 2016) and weak wind shear (Fan et al., 2009, 2012b, 2013; Li et al., 2008; Lebo et al., 2012). Grabowski and Morrison (2016; 2020) argued this invigoration does not exist because the increase in the buoyancy by freezing is completely offset by the buoyancy for carrying the extra cloud water across the freezing level. However, Rosenfeld

54   et al. (2008) showed that the buoyancy restores and increases after the precipitation of the ice

55   hydrometeors that form upon freezing of the high supercooled liquid water content into large

56   graupel and hail.

57   Another theory is that increasing aerosols enhances droplet nucleation particularly secondary

58   nucleation after warm rain initiates, which promotes condensation because of larger integrated

59   droplet surface area associated with a higher number of small droplets (Fan et al., 2007, 2013,

60   2018; Koren at al., 2014; Lebo, 2018; Sheffield et al., 2015; Chen et al., 2020). This so-called

61   "warm-phase invigoration", which is manifested in a warm, humid, and clean environment under

62   which the addition of a large number of ultrafine aerosol particles from urban pollution leads to

63   stronger invigoration than the "cold-phase invigoration" (Fan et al., 2018). Grabowski and

64   Morrison (2020) proposed a different interpretation of the warm-phase invigoration from the

65   literature listed above. They argued that condensation rates only depend on updraft velocity with

66   the quasi-steady assumption (i.e., the true supersaturation is approximated with the equilibrium

67   supersaturation), therefore they interpreted that it is the lower equilibrium supersaturation in

68   polluted conditions that lead to a larger buoyancy, thus enhanced updraft speeds, and condensation.

69   Several studies showed that the quasi-steady assumption is invalidated in the conditions of low

70   droplet concentrations (Politovich and Cooper, 1988; Korolev and Mazin, 2003) or acceleration of

71   vertical velocity (Pinsky et al., 2013).

72   Many factors can affect whether aerosols invigorate or suppress convective intensity through

73   ACI, such as environmental wind shear (Fan et al., 2009; Lebo et al., 2012), relative humidity (Fan

74   et al., 2007; Khain et al., 2008), and Convective Available Potential Energy (Lebo et al., 2012;

75   Morrison, 2012; Storer et al., 2010). Meteorological buffering effects were also found for aerosol

76   effects on convective clouds over a large region and long-time (over a few days and weeks)

77 simulations (Stevens and Feingold, 2009; van den Heever et al., 2011). Dagan et al. (2018) showed

78 that the lifetimes of cloud systems are mostly much shorter than that and rarely reach this buffering

79 state. For DCCs with complicated dynamics, thermodynamics, and microphysics, aerosol impacts

80 are extremely complex and remain poorly known. Confidently isolating and quantifying an aerosol

81 deep convective invigoration effect from observations requires very long-term measurements: data

82 of 10 years are still not enough over the Southern Great Plains due to the large variability of

83 meteorological conditions (Varble, 2018).

84   Modeling of ACI is quite dependent on cloud microphysics parameterization schemes (e.g.,

85 Fan et al., 2012a; Khain and Lynn, 2009; Khain et al., 2009, 2015; Lebo and Seinfeld, 2011; Lee

86 et al., 2018; Loftus and Cotton, 2014; Wang et al., 2013). Two-moment bulk and bin schemes have

87 been widely used in ACI studies (e.g., Chen et al., 2011; Fan et al., 2013; Khain et al., 2010). In

88 two-moment bulk schemes, hydrometeor size distributions are diagnosed from the predicted

89 number and mass with an assumed spectral shape (e.g., gamma function). The saturation

90 adjustment approach is often used for calculating condensation and evaporation, meaning

91 supersaturation and undersaturation with respect to water are removed in the cloud within a

92 timestep. Some bulk schemes take the explicit supersaturation approach to allow supersaturation

93 to evolve (e.g., Morrison and Grabowski, 2007; 2008). In bin schemes, the size distributions of

94 hydrometeors are discretized by a number of size bins and predicted, which represents some

95 aerosol-cloud interaction processes more physically compared with bulk schemes (Fan et al., 2016;

96 Khain et al., 2015). Supersaturation is generally predicted in bin schemes.

97   Many studies have shown that bulk schemes are limited in representing certain important

98 microphysical processes such as aerosol activation, condensation, deposition, sedimentation, and

99 rain evaporation (Ekman et al., 2011; Khain et al., 2009; Lee et al. 2018; Li et al., 2009; Milbrandt

100 and Yau, 2005; Morrison, 2012; Wang et al., 2013). Though bin cloud microphysics can provide

101 a more rigorous numerical solution and a more robust cloud microphysics representation than

102 typical bulk microphysics, it is often applied in simulations for process understanding but rarely

103 in operational applications due to the expensive computation cost. For not introducing further

104 computation cost, bin schemes are also often run with a prescribed aerosol spectrum assuming a

105 fixed composition and a simple aerosol budget treatment without coupling with chemistry/aerosol

106 calculations. As a result, many aerosol life cycle processes such as aerosol nucleation, growth,

107 aqueous chemistry, aerosol resuspension, and below-cloud wet removal are missing or crudely

108 parameterized. Therefore, it is difficult to simulate the spatial and temporal variabilities of aerosol

109 chemical composition and size distribution. In Gao et al. (2016), we have coupled a spectral-bin

110 microphysics scheme (SBM; Fan et al., 2012a; Khain et al., 2004) with the Chemistry version of

111 the Weather Research and Forecast model (WRF-Chem; Grell et al., 2005; Skamarock et

112 al., 2008), called WRF-Chem-SBM, to address above-mentioned limitations. In this new model,

113 the SBM was coupled with the Model for Simulating Aerosol Interactions and Chemistry

114 (MOSAIC; Fast et al., 2006; Zaveri et al., 2008). The newly coupled system was initially evaluated

115 for warm marine stratocumulus clouds and showed a much-improved simulation of cloud droplet

116 number concentration and liquid water content compared with the default Morrison two-moment

117 bulk scheme (Gao et al., 2016).

118   The Houston area in summer, where isolated convective clouds with very warm cloud-bases

119 often occurred in the afternoon (Yuan et al., 2008), offers (a) a combination of polluted aerosols

120 from the urban and industrial area of Houston with significantly low background aerosol

121 concentrations surrounding Houston, (b) aerosol sources that are not correlated with meteorology,

122 and (c) weak synoptic forcing along with strong local triggering in the form of land-sea contrasts

123 and sea breeze fronts. This combination allows the manifestation of potentially large aerosol

124 effects. In this study, we choose a sea-breezed induced DCC case occurring 19-20 June 2013 near

125 Houston to (1) evaluate the performances of WRF-Chem-SBM in simulating deep convective

126 clouds and (2) gain a better understanding of the differences in aerosol effects predicted by SBM

127 and the Morrison two-moment bulk scheme as well as the major factors/processes responsible for

128 the differences. Considering that the convective clouds over the Houston area are mainly impacted

129 by the aerosols produced from anthropogenic activities, we focus on the anthropogenic aerosol

130 effect in this study. The simulated storm case is the same as the case for the Aerosol-Cloud-

131 Precipitation-Cloud (ACPC) Model Intercomparison Project (Rosenfeld et al., 2014;

132 www.acpcinitiative.org).

2 Case Description and Observational Data

134 The deep convective cloud event that we simulate in this study occurred on 19-20 June 2013

135 near Houston, Texas. The isolated relatively weak convective clouds started in the late morning

136 because of a trailing front. With increased solar radiation in the early afternoon and strengthening

137 of a sea breeze circulation that transports warm and humid air from the Gulf of Mexico to the

138 Houston urban area, deep convective cells over Houston and Galveston bay areas developed (Fig.

139 1). The strong convective cell observed near the Houston city was initiated around 2145 UTC

140 (local time 16:45) and developed to its peak precipitation at 2217 UTC based on radar observation

141 (Fig. 1). The maximum reflectivity was more than 55 dBZ. This storm cell lasted for about 1.5

142 hours.

143 We used the following observation data for model evaluation. Particulate matter (PM) 2.5

144 data provided by Texas Commission for Environmental Quality (TCEQ) at

145 https://www.tceq.texas.gov/agency/data/pm25.html are used to evaluate the simulated aerosols

146 near the surface. The data for evaluating cloud base heights and CCN number concentration at

147 cloud base are obtained from the Visible Infrared Imaging Radiometer Suite (VIIRS) retrievals

148 based on the method of Rosenfeld et al., (2016). The 2-m temperature and 10-m winds are from

149 the North American Land Data Assimilation System (NLDAS) with 0.125-deg resolution at

150 https://climatedataguide.ucar.edu/climate-data/nldas-north-american-land-data-assimilation-

151 system. The observed radar reflectivity is used to evaluate the simulated convective system. The

152 radar reflectivity is obtained from Next-Generation Weather Radar (NEXRAD) network at

153 https://www.ncdc.noaa.gov/data-access/radar-data/nexrad-products, with a temporal frequency of

154 every ~ 5 minutes and 1 km horizontal spatial resolution.

155 **3. Model description and experiments**

156   We conducted model simulations using the version of WRF-Chem based on Gao et al.

157 (2016) coupling with the Morrison two-moment scheme (Morrison et al., 2005; Morrison et al.,

158 2009; Morrison and Milbrandt, 2011) and SBM (Khain et al., 2004; Fan et al., 2012). The version

159 of SBM employed in this study is a fast version of the Hebrew University Cloud Model (HUCM)

160 described by Khain et al. (2004) with improvements from Fan et al. (2012a) and (2017). The

161 considered hydrometer size distributions are droplets/raindrops, cloud ice/snow, and graupel. The

162 graupel version is used because it is more appropriate for simulating the convective storm over the

163 Houston area than the hail version. SBM is currently coupled with the four-sector version of

164 MOSAIC (0.039-0.156, 0.156-0.624, 0.624-2.5 and 2.5-10.0 μm). As detailed in Gao et al. (2016),

165 the aerosol processes including aerosol activation, resuspension, and in-cloud wet-removal are also

166 improved. Theoretically, both aerosol and cloud processes can be more realistically simulated

167 particularly under the conditions of complicated aerosol compositions and aerosol spatial

168 heterogeneity compared with original WRF-Chem. The dynamic core of WRF-Chem-SBM is the

169   Advanced Research WRF model that is fully compressible and non-hydrostatic with a terrain-

170   following hydrostatic pressure vertical coordinate (Skamarock et al., 2008). The grid staggering is

171   the Arakawa C-grid. The model uses the Runge-Kutta 3rd order time integration schemes, and the

172   3rd and 5th order advection schemes are selected for the vertical and horizontal directions,

173   respectively. The positive-definite option is employed for the advection of moist and scalar

174   variables.

175   Two nested domains with horizontal grid spacings of 2 and 0.5 km and horizontal grid points

176   of 450×350 and 500×400 for Domain 1 and Domain 2, respectively, are used (Fig. 2a), with 51

177   vertical levels up to 50 hPa which allows about 50-100 m grid spacings below 2-km altitude and

178   ~500 m above it. The simulations for Domain 1 and Domain 2 are run separately and the Domain

179   1 simulations serve to provide the chemical and aerosol lateral boundary and initial conditions of

180   Domain 2. The chemical and aerosol lateral boundary and initial conditions for Domain 1

181   simulations were from a quasi-global WRF-Chem simulation at 1-degree grid spacing, and

182   meteorological lateral boundary and initial conditions were created from MERRA-2 at the grid

183   spacing of $0.5° \times 0.625°$ (Gelaro et al., 2017). Two simulations were run over Domain 1 with

184   anthropogenic emissions turned on and off, respectively, to provide two different aerosol scenarios

185   for the initial and boundary chemical and aerosol conditions for Domain 2 simulations: (1) a

186   polluted aerosol scenario with anthropogenic aerosols accounted which is for the real situation; (2)

187   an assumptive clean scenario without anthropogenic aerosols. Domain 2 is run with initial and

188   lateral boundary chemical and aerosols fields from Domain 1 outputs and initial and lateral

189   boundary meteorological conditions from MERRA-2. Note that we use the meteorology from

190   MERRA-2 as the initial and lateral boundary conditions for Domain 2 instead of Domain 1 outputs,

191   because we want to keep the initial and lateral boundary meteorological conditions the same for

192 all the sensitivity tests with different microphysics and aerosol setups (meteorology is different

193 between the two simulations over Domain 1).

194   The simulations in Domain 1 were initiated at 0000 UTC on 14 Jun and ended at 1200 UTC

195 on 20 June with about 5 days for the chemistry spin-up. The meteorological fields were

196 reinitialized every 36 hours to prevent the model from drifting. The dynamic time step was 6 s for

197 Domain 1 and 3 s for Domain 2. The anthropogenic emission was from NEI-2011 emissions. The

198 biogenic emission came from the Model of Emissions of Gases and Aerosols from Nature

199 (MEGAN) product (Guenther et al., 2006). The biomass burning emission was from the Fire

200 Inventory from NCAR (FINN) model (Wiedinmyer et al., 2011). We used the Carbon Bond

201 Mechanism Z (CBMZ) gas-phase chemistry (Zaveri and Peters, 1999) and MOSAIC aerosol

202 model with four bins (Zaveri et al., 2008). The physics schemes other than microphysics applied

203 in the simulation are the Unified Noah land surface scheme (Chen and Dudhia, 2001), Mellor-

204 Yamada-Janjic planetary boundary layer scheme (Janjic et al., 1994), Multi-layer, Building

205 Environment Parameterization (BEP) urban physics scheme (Salamanca and Martilli, 2010), the

206 RRTMG longwave and shortwave radiation schemes (Iacono et al., 2008).

207   The main purpose of the simulations in Domain 1 is to provide initial and boundary chemical

208 and aerosol conditions for the simulations in Domain 2. To save computational cost, WRF-Chem

209 coupled with Morrison two-moment bulk microphysics scheme (Morrison et al., 2005) is used for

210 the simulations in Domain 1. Two simulations run for Domain 1 are referred to as D1_MOR_anth

211 in which the anthropogenic emissions are turned on and D1_MOR_noanth where the

212 anthropogenic emissions are turned off. Then four major experiments are carried out to simulate

213 the convective event near Houston over Domain 2 with two cloud microphysics schemes and two

214 aerosol scenarios, respectively. We refer to the simulation in which SBM is used and the

215   anthropogenic emissions are included using the initial and boundary chemicals and aerosols from

216   D1_MOR_anth, as our baseline simulation (referred to as "SBM_anth"). SBM_noanth is based on

217   SBM_anth but uses initial and boundary chemicals and aerosols from D1_MOR_noanth and turns

218   off the anthropogenic emissions, meaning that anthropogenic aerosols are not taken into account.

219   MOR_anth and MOR_noanth are the two corresponding simulations to SBM_anth and

220   SBM_noanth, respectively, using the Morrison two-moment bulk microphysics scheme.

221   The SBM and Morrison schemes are two completely different representations of cloud

222   microphysics so they are different in many aspects including major microphysical processes such

223   as aerosol activation, condensation/evaporation, collisions, and ice nucleation and ice growth

224   through riming and aggregation. Details are read from Khain et al. (2004; 2015), Morrsion et al.

225   (2015), and Gao et al. (2016). The calculations of aerosol activation and condensation/evaporation

226   in the SBM scheme are based on the Köhler theory and diffusional growth equations in light of

227   particle size and supersaturation, receptively. Whereas in WRF-Chem with the Morrison scheme,

228   the Abdul-Razzak and Ghan (2002) parameterization is used for aerosol activation and the

229   saturation adjustment method is applied for condensation and evaporation calculation. To examine

230   the contribution of the saturation adjustment approach for condensation and evaporation to the

231   simulated aerosol effects with the Morrison scheme, we further conducted two sensitivity tests,

232   based on MOR_anth and MOR_noanth, by replacing the saturation adjustment approach in the

233   Morrison scheme with the condensation and evaporation calculation based on an explicit

234   representation of supersaturation over a time step as described in Lebo et al. (2012). That is, the

235   supersaturation is solved semi-analytically based on both the forcing from advection and the

236   microphysics processes. Note in both SBM and this modified Morrison scheme, the

237   supersaturation for condensation and evaporation is calculated after the advection. These two

238   simulations are referred to as MOR_SS_anth and MOR_SS_noanth, respectively. To present more

239   robust results, we carry out a small number of ensembles (three) for each case over Domain 2 (we

240   do not have computer time to do more ensemble runs). The three ensemble runs are only different

241   in the initialization time: 0000 UTC, 0600 UTC, and 1200 UTC on 19 June. All the simulations

242   end at 1200 UTC on 20 June. The analysis results for Domain 2 simulations in this study are based

243   on the mean values of three ensemble runs and the ensemble spread is shown as the shaded area

244   in all profile figures.

245   We evaluate the aerosol and CCN properties simulated by D1_MOR_anth to ensure realistic

246   aerosol fields, which are used for the Domain 2 simulations with anthropogenic aerosols

247   considered. These evaluations are included in section 4.1.

248   From D1_MOR_anth, we see a very large spatial variability of aerosol number concentrations

249   (Fig. 2b). There are three regions with significantly different aerosol loadings over the domain as

250   shown by the black boxes in Fig. 2b: (a) the Houston urban area, (b) the rural area about 100 km

251   northeast of Houston, and (c) the Gulf of Mexico. Aerosols over the Houston urban area are mainly

252   contributed by organic aerosols, which are highly related to industrial and ship channel emissions.

253   The rural area aerosols are mainly from sulfate and sea salt aerosol is the major contributor over

254   the Gulf of Mexico. This suggests that aerosol properties are extremely heterogeneous in this

255   region. The aerosols over Houston urban area are generally about 5 and 10 times higher than the

256   rural and Gulf area, respectively (Fig. 2c). The size distributions show a three-mode distribution

257   with the largest differences from the Aitken mode (peaks at 50 nm; Fig. 2c). These ultrafine aerosol

258   particles are mainly contributed by anthropogenic activities (Fig. 2b, d). With the anthropogenic

259   emissions turned off, the simulated aerosols are much lower and have much less spatial variability

260   (Fig. 2d).

4 Results

4.1 Model Evaluation

We first show the evaluation of the aerosol and CCN properties simulated by D1_MOR_anth, which runs over Domain 1, much larger than Domain 2. As described in Table 1, there are eight PM monitoring sites from TCEQ around the Houston area. Surface PM2.5 shows high concentrations at Houston and its downwind regions (Fig. 3). D1_MOR_anth shows a similar spatial pattern with the observations in terms of the surface PM2.5 averaged over 24 hours (the day before the convection near Houston), although with a difficulty to reproduce the values for some sites. The hourly variations of ground-level PM2.5 concentrations from both observation and D1_MOR_anth for these sites in the day before the convective initiation are depicted in Fig. 4. Generally, the simulated hourly pattern agrees with the observation for eight stations. D1_MOR_anth reproduces the diurnal variations, especially the increasing trend from 1200 UTC to 1800 UTC 19 Jun prior to the initiation of deep convective cells over Houston and Galveston bay areas.

The evaluation of the cloud base heights and CCN at cloud bases at the warm cloud stage before transitioning to deep clouds (2000 UTC) are shown in Fig.5. Over Houston and its surrounding area (black box in Fig. 5), the simulated cloud base heights are about 1.5-2 km, in agreement with the retrieved values from VIIRS satellite, which are around 1.2-1.8 km (Fig. 5a-b). The retrieved CCN concentrations at cloud bases vary significantly over the domain and this spatial variability is generally captured by the model (Fig. 5c-d). For example, D1_MOR_anth simulates some high CCN concentrations (400-800 cm^{-3} with some above 1000 cm^{-3}) over the Houston and around the Bay area, relatively low CCN values in the rural areas (about 200-600 cm^{-} ^{3}), and very low values over the Gulf of Mexico (less than 200 cm^{-3}), as shown in Fig. 5d. This is

13

284   consistent with the spatial variability from the retrievals (Fig. 5c). The evaluation of aerosol

285   properties before the initiation of Houston convective cells and CCN at the warm cloud stage

286   before transitioning to deep clouds provides us confidence in using the chemical and aerosol fields

287   from Domain 1 outputs to feed Domain 2 simulations.

288   Now we are evaluating near-surface temperature and winds, reflectivity, and precipitation

289   simulated by SBM_anth and MOR_anth. Fig. 6 shows the comparisons in 2-m temperature and

290   10-m winds at 1800 UTC (before the convective initiation). Compared with the coarse resolution

291   NLDAS data, both SBM_anth and MOR_anth capture the general temperature pattern with a little

292   overestimation in the northeast part of the domain (mainly rural area). The modeled southerly

293   winds do not reach further north as the NLDAS data, possibly because of the feedback of the small-

294   scale features which are simulated with the high resolution to mesoscale circulations. However,

295   the simulation of temperature over Houston and sea breeze winds from the Gulf of Mexico to

296   Houston is the most important in this case. SBM_anth predicts a slightly higher temperature than

297   MOR_anth in the northern part of the Houston region (purple box in Fig. 6), which agrees with

298   NLDAS better. SBM_anth gets similar southerly winds from the Gulf of Mexico to Houston as

299   shown in NLDAS, while the southerly winds from the Gulf of Mexico become very weak or

300   disappear prior to reaching Houston in MOR_anth.

301   For the Houston convective cell that we focused (red box in Fig. 7a), SBM_anth simulates

302   it well in both locations and high reflectivity value (greater than 50 dBZ) in comparison with the

303   NEXRAD observation (Fig. 7a, b, d, f). The simulated composite reflectivities (i.e., the column

304   maximum) are up to 55-60 dBZ from all three ensemble members, consistent with NEXRAD.

305   With the Morrison scheme, MOR_anth simulates several small convective cells near Houston with

306   a maximum reflectivity of 55 dBZ or less (Fig. 7c, e, g). All three ensemble members consistently

307   show smaller but more scattered convective cells with the Morrison scheme compared with SBM.

308   The contoured frequency by altitude diagram (CFAD) plots for the entire storm period show that

309   SBM_anth is in better agreement with observation compared with MOR_anth, especially for the

310   vertical structure of the high reflectivity range (greater than 48 dBZ, black dashed lines in Fig. 8)

311   and echo top heights, which can reach up to 14-15 km (Fig. 8a-b). MOR_anth overestimates the

312   occurrence frequencies of the 35-45 dBZ range and underestimates those of the low and high

313   reflectivity ranges (less than 15 dBZ or larger than 50 dBZ) as well as the echo top heights (1-2

314   km lower than SBM_anth; Fig. 8c).

315   For the precipitation rates averaged over the study area (red box in Fig. 7), the observation

316   shows two peaks, which are captured by both SBM_anth and MOR_anth (Fig. 9a). However, the

317   timing for the first peak is about 30 and 60 min earlier in SBM_anth and MOR_anth than the

318   observation, respectively. Also, SBM_anth predicts the rain rate intensities at the two peak times

319   more consistent with the observations whereas MOR_anth underestimates the rain rate intensity at

320   the second peak time (Fig. 9a). The large precipitation rates (greater than 15 mm h^{-1}) in SBM_anth

321   has a ~1.5 times larger occurrence probability than those in MOR_anth, showing a better

322   agreement with the observation (Fig. 9b). The observed accumulated rain over the time period

323   shown in Fig. 9a is about 3.8 mm, and both SBM_anth (~ 4.5 mm) and MOR_anth (~ 4.2 mm)

324   overestimate the accumulated precipitation due to the longer rain period compared with the

325   observations. Overall, the performance of SBM_anth is superior to MOR_anth in simulating the

326 location and intensity of the convective storm and associated precipitation by comparing with the

327 observation.

4.2 Simulated Aerosol Effects on Cloud and Precipitation

329   Now we look at the effects of anthropogenic aerosols on the deep convective storm

330 simulated with SBM and Morrison microphysics schemes. Fig. 9a shows that with the SBM

331 scheme, anthropogenic aerosols remarkably increase the mean surface rain rates (by ~30%; from

332 SBM_noanth to SBM_anth), mainly because of the increased occurrence frequency (nearly

333 doubled) for relatively large rain rates (i.e., 10-15 mm h^{-1} and >15 mm h^{-1}) in Fig. 9b. With the

334 Morrison scheme, the changes in mean precipitation and the PDF from MOR_noanth to

335 MOR_anth are relatively small, showing a very limited aerosol effect on precipitation. Both SBM

336 and Morrison schemes show higher occurrences of large precipitation rates (> 10 mm h^{-1}) and

337 lower occurrences of small precipitation rates (< 10 mm h^{-1}) due to anthropogenic aerosols (Fig.

338 9b), but the effect is larger with SBM. For the accumulated precipitation, the anthropogenic

339 aerosols lead to a ~ 0.5 mm increase over the storm period with the SBM scheme, while only a ~

340 0.2 mm increase with the Morrison scheme. Note Fig. 9a shows that anthropogenic aerosols lead

341 to an earlier start of the precipitation with both SBM and Morrison, which reflects the faster

342 transition of warm rain to mixed-phase precipitation. We do see the delay of warm rain by aerosols

343 but only about 5 min (probably due to the humid condition of the case), which is difficult to be

344 shown in Fig. 9a since the averaged rain rate for the analysis box is ~ 0.02 mm hr^{-1} and the time

345 period is very short (~ 10 min).

346   With the SBM scheme, the increase in the updraft speeds by the anthropogenic aerosols is

347 even more notable than the precipitation (Fig. 10a-b). Above 5-km altitude, the occurrence

348 frequencies of updraft speed greater than 0.4% extend to much larger values, with 36 m s^{-1} at the

349   upper levels in SBM_anth while only ~ 20 m s^{-1} in SBM_noanth. With the Morrison scheme, the

350   changes are not significant by the anthropogenic aerosols (MOR_noanth vs MOR_anth in Fig.

351   10c-d). From MOR_noanth to MOR_anth, there is a slight increase in updraft speed at around 9-

352   11 km altitudes but a slight decrease at 6-8 km altitudes. The significant invigoration of convective

353   intensity by anthropogenic aerosols with the SBM scheme explains the much larger occurrences

354   of relatively large rain rates and overall more surface precipitation due to the anthropogenic aerosol

355   effect (Fig. 9).

356   Now the question is why the anthropogenic aerosols enhance the convective intensity of

357   the storm with the SBM scheme while the effect is very small with the Morrison scheme. Fig. 11

358   shows the vertical profiles of mean updraft velocity, buoyancy, and total latent heating rate of the

359   top 25th percentile updrafts with a value greater than 2 m s^{-1} during the deep convective cloud

360   stage. Both SBM and MORR show similar vertical structures of convective intensity but the

361   convective intensity with the Morrison scheme is weaker than SBM in the case with anthropogenic

362   aerosols considered, especially at high altitudes. With the SBM microphysics scheme, the

363   increased convective intensity due to the anthropogenic aerosol effect corresponds to the increased

364   buoyancy (~ 30%) from SBM_noanth to SBM_anth (Fig. 11a, c). The increased buoyancy can be

365   explained by the increased total latent heating (Fig. 11e). From SBM_noanth to SBM_anth, the

366   increase in latent heating from both condensation and ice-related microphysical processes

367   (including deposition, drop freezing, and riming) is significant, with the increase from

368   condensation latent heating is relatively larger (about 60% more as shown in Fig. 12a). As shown

369   in Fan et al., (2018), the increase in lower-level condensation latent heating has a much larger

370   effect on intensifying updraft intensity compared with the same amount of increase in high-level

371   latent heating from ice-related microphysical processes. Thus, the convective invigoration by the

17

372 anthropogenic aerosols with the SBM scheme is through both warm-phase invigoration and cold-

373 phase invigoration, with the former playing a more important role. Compared with the Morrison

374 scheme, the increase of total latent heating by the anthropogenic aerosols is almost doubled with

375 the SBM scheme, explaining more remarkable enhancement of buoyancy and thus the convective

376 intensity (red lines vs blue lines in Fig. 11). From MOR_noanth to MOR_anth, there is a small

377 increase in both the condensation latent heating and high-level latent heating associated with ice-

378 related processes (blue lines in Fig. 12b). As shown in Fig. 12, the difference in the increase of

379 latent heating by the anthropogenic aerosols between SBM and Morrison schemes comes from

380 both condensation latent heating (with a ~ 20% increase with SBM but only ~ 8% with Morrison)

381 and ice-related processes latent heating (with a ~ 13% increase with SBM and ~ 10% with

382 Morrison), with the major differences from condensation latent heating. The small increase in

383 condensation latent heating limits convective invigoration by aerosols with the Morrison scheme.

384   To understand why the responses of condensation to the anthropogenic aerosols are

385 different between the SBM and Morrison schemes, we look into the process rates of drop

386 nucleation and condensation (Fig. 13). With the SBM scheme, the anthropogenic aerosols increase

387 the drop nucleation rates by a few times over the profile (red lines in Fig. 13a), and the

388 condensation rates (i.e., the rate of gain in cloud water due to water vapor condensation) are also

389 drastically increased (doubled between 4-6 km altitudes as shown in Fig. 13c). The enhanced

390 condensation rate by the anthropogenic aerosols is because much more aerosols are activated to

391 form a larger number of small droplets, increasing the integrated droplet surface area for

392 condensation, as documented in Fan et al., (2018). As a result, supersaturation is drastically lower

393 in SBM_anth than SBM_noanth (green lines in Fig. 13a). With the Morrison scheme, similarly to

394 SBM, a large increase in the droplet nucleation rate is seen (Fig. 13b). However, the condensation

395   rates are barely increased (blue solid vs. dashed lines in Fig. 13d). We hypothesize that the lack of

396   response of condensation to the increased aerosol activation with the Morrison scheme is mainly

397   because of the saturation adjustment calculation of the condensation and evaporation process. The

398   approach does not allow supersaturation in the cloud and the calculation of condensation does not

399   depend on supersaturation and droplet properties, thus removes the sensitivity to the anthropogenic

400   aerosols.

401   To verify our hypothesis and examine how much the saturation adjustment method is

402   responsible for the weak responses of condensation latent heating and convection to the added

403   anthropogenic aerosols, we conducted two additional sensitivity tests by replacing the

404   saturation adjustment approach in the Morrison scheme with the condensation and evaporation

405   calculation based on an explicit representation of supersaturation over a time step, as described in

406   Section 3. The result shows that the modified Morrison scheme with the explicit supersaturation

407   leads to (1) larger condensation rates and latent heating (Figs. 12b and 13d) and (2) a larger

408   anthropogenic aerosol effect on condensation and ice-related processes, compared with the

409   saturation adjustment approach.

410   First, we explain why the explicit supersaturation leads to larger condensation rates and

411   latent heating than the saturation adjustment. The time evolution of latent heating, updraft, and

412   hydrometeor properties is examined (Fig. S1). At the warm cloud stage at 1700 UTC, the saturation

413   adjustment produces more condensation latent heating which leads to larger buoyancy and stronger

414   updraft intensity compared to the explicit supersaturation because of removing supersaturation

415   (Fig. S1, left, blue vs. orange). However, by the time of 1900 UTC when the clouds have developed

416   into mixed-phase clouds, the saturation adjustment produces smaller condensational heating and

417   weaker convection than the explicit supersaturation approach (Fig. S1, middle). The results remain

418   similarly later at the deep cloud stage 2100 UTC (Fig. S1, right). How does this change happen

419   from 1700 to 1900 UTC? At the warm cloud stage (1700 UTC), the saturation adjustment produces

420   droplets with larger sizes (up to 100% larger for the mean radius) than the explicit supersaturation

421   because of more cloud water produced as a result of zeroing-out supersaturation at each time step

422   (droplet formation is similar between the two cases as shown in Fig. 13). This results in much

423   faster and larger warm rain, while with the explicit supersaturation rain number and mass are

424   absent at 1700 UTC as shown in Fig. S2d and S3d). As a result, when evolving into the mixed-

425   phase stage (1900 UTC), much fewer cloud droplets are transported to the levels above the freezing

426   level (Fig. S2b and S3b). Whereas with the explicit supersaturation, because of the

427   delayed/suppressed warm rain and smaller droplets (the mean radius is decreased from 8 to 6 μm

428   at 3 km), much more cloud droplets are lifted to the higher levels. Correspondingly, a few times

429   higher total ice particle number and mass are seen compared with the saturation adjustment (Fig.

430   S2g and S3g) because more droplets above the freezing level induce stronger ice processes (droplet

431   freezing, riming, and deposition). This leads to more latent heat release (Fig. S1e), which increases

432   the buoyancy and convective intensity. When convection is stronger, more condensation occurs

433   thus a larger condensation latent heating is seen with the explicit supersaturation.

434   Now we explain why the explicit supersaturation leads to a larger aerosol effect on

435   convective intensity compared with the saturation adjustment approach. First, the enhancement of

436   condensational heating is larger by aerosols with the explicit supersaturation (Fig. S1a-c), mainly

437   because the condensation depends on supersaturation and droplet properties, while the saturation

438   adjustment approach removes the dependence of condensation on droplet properties. Second,

439   increasing aerosols with the explicit supersaturation leads to a larger enhancement of ice-related

440   processes (Fig. S1b-c) due to a larger reduction in droplet size (up to 1 μm more in the mean radius)

441   than the saturation adjustment. The enhanced convective intensity would further lead to a larger

442   enhancement in condensational heating. Therefore, we see a much larger aerosol effect with the

443   explicit supersaturation than with the saturation adjustment because of more enhanced

444   condensation latent heating and ice-related latent heating. The increase in condensation latent

445   heating and ice-related latent heating by the anthropogenic aerosols with explicit supersaturation

446   is comparable to SBM (orange lines vs red lines in Figure 12), resulting in a similarly large increase

447   in buoyancy and thus convective intensity (orange lines vs red lines in Fig. 11). The increase of

448   precipitation by aerosols is also similar to that with the SBM scheme (not shown).

449   With enhanced convection by anthropogenic aerosols, the responses of hydrometeor mass

450   and number are significant. With the SBM scheme, the increases in mass and number of cloud

451   droplets, raindrops, and total ice particles (ice, snow, and graupel) by the anthropogenic aerosols

452   are very significant (Fig. 14-15, left, red lines). The increases in the total ice mass and number are

453   particularly significant ($\sim 35\%$ in mass and $\sim 30\%$ in number). The mass increase in frozen

454   hydrometeors is mainly contributed by graupel (Fig. S4, left, red lines) while the number increase

455   mainly comes from cloud ice (Fig. S5, red lines). This suggests a large effect of enhanced

456   convective intensity on frozen hydrometeors and thus precipitation. With the Morrison scheme,

457   little change is seen (Fig. 14-15 and Fig. S4-S5, right, blue lines). By replacing the saturation

458   adjustment with the explicit supersaturation for condensation and evaporation, the increases in

459   those hydrometeor masses and numbers become consistent with the SBM scheme (Fig. 14-15 and

460   Fig. S4-S5, orange lines and red lines).

461   These results verify that the saturation adjustment approach for parameterizing

462   condensation and evaporation is the major reason responsible for limited aerosol effects on

463   convective intensity and precipitation with the original Morrison scheme. Past studies also showed

464   the limitations of the saturation adjustment approach in simulating aerosol impacts on deep

465   convective clouds (e.g., Fan et al., 2016; Lebo et al., 2012; Lee et al., 2018; Wang et al., 2013).

5 Conclusions and Discussion

467   We have conducted model simulations of a deep convective cloud case occurring on 19 June

468   2013 over the Houston area with WRF-Chem coupled with the SBM and Morrison microphysics

469   schemes to (1) evaluate the performance of WRF-Chem-SBM in simulating the deep convective

470   clouds, and (2) explore the differences in aerosol effects on the deep convective clouds produced

471   by the SBM and Morrison schemes and the major factors responsible for the differences.

472   We have evaluated the simulated aerosols, CCN, cloud base heights, reflectivity, and

473   precipitation. The model simulates the large spatial variability of aerosols and CCN from the Gulf

474   of Mexico, rural areas, to Houston city. On the bulk magnitudes, the model captures the surface

475   PM2.5, cloud base height, and CCN at cloud bases near Houston reasonably well. These

476   realistically simulated aerosol fields were fed to higher resolution simulations (0.5 km) using the

477   SBM and Morrison schemes. With the SBM scheme, the model simulates a deep convective cloud

478   over Houston in a better agreement with the observed radar reflectivity and precipitation,

479   compared with using the Morrison scheme. Indeed, both schemes show similar vertical structures

480   of convective intensity and hydrometeor properties, with a weaker updraft intensity with the

481   Morrison scheme at high altitudes in the case with anthropogenic aerosols considered.

482   Replacing the saturation adjustment for the condensation and evaporation calculation with an

483   explicit supersaturation approach leads to an increase in updraft intensity, resulting in similar

484   results as SBM for the case with anthropogenic aerosols considered. This is because with the

485   explicit supersaturation approach droplet sizes are smaller in the warm cloud stage than the

486   saturation adjustment which removes supersaturation within one timestep. The less efficient

22

487   conversion of cloud droplets to rain allows more cloud droplets to be transported to the altitudes

488   above the freezing level at the mixed-phase and deep cloud stages, inducing stronger ice

489   microphysical processes (freezing, riming, and deposition) and invigorating convection. Lebo et

490   al. (2012) showed a similar feature that the saturation adjustment has a larger total condensate

491   mass at the beginning but less at the later stage compared to the explicit supersaturation approach,

492   particularly in total ice mass. In addition, Grabowski and Morrison (2017) showed that the

493   saturation adjustment affected ice processes in another way by producing larger ice particles with

494   larger falling velocities compared with the explicit supersaturation approach, leading to the

495   reduction of anvil clouds.

496   About the anthropogenic aerosol effects, with the SBM scheme, anthropogenic aerosols

497   notably increase the convective intensity, enhance the peak precipitation rate over the Houston

498   area (by $\sim$ 30%), and double the frequencies of relatively large rain rates (> 10 mm h^{-1}). The

499   enhanced convective intensity by anthropogenic aerosols makes the simulated storm agree better

500   with the observed, mainly attributed to the increased condensation and ice-related latent heating,

501   with the former is more significant. In contrast, with the Morrison scheme, there is no significant

502   anthropogenic aerosol effect on the convective intensity and total precipitation. But the Morrison

503   schemes indeed shows qualitatively consistent results with SBM in aerosol effects on the PDF of

504   rain rates: higher occurrences of large precipitation rates (> 10 mm h^{-1}) and lower occurrences of

505   small precipitation rates (< 10 mm h^{-1}).

506   By replacing the saturation adjustment with an explicit supersaturation approach for the

507   condensation and evaporation calculation, the modified Morrison shows much larger

508   anthropogenic aerosol effects on convective intensity, hydrometeor properties, and precipitation

509   than the original Morrison scheme, and those aerosol effects are similar to the SBM scheme.

510 Therefore, the saturation adjustment method for the condensation and evaporation calculation is

511 mainly responsible for the limited aerosol effects with the Morrison scheme. This is mainly

512 because the saturation adjustment approach limits the enhancement in (1) condensation latent heat

513 by removing the dependence of condensation on droplets/aerosols and (2) the ice-related processes

514 because the approach leads to stronger warm rain and weaker ice processes than the explicit

515 supersaturation approach. Therefore, the explicit supersaturation enhances aerosol effects through

516 enhanced condensation and cold-phase processes, but enhanced condensation should play a more

517 important role. This study suggests, when the computational resource is not sufficient or in other

518 situations such as the application of SBM is not available, the Morrison scheme modified with the

519 condensation and evaporation calculation based on a simple representation of supersaturation can

520 be applied to study aerosol effects on convective clouds, especially for warm and humid cloud

521 cases in which the response of condensation to aerosols is particularly important.

522 Following Fan et al., (2018), which showed that the warm-phase invigoration mechanism

523 was manifested by ultrafine aerosol particles in the Amazon warm and humid environment with

524 extremely low background aerosol particles. Here we showed that in summer anthropogenic

525 aerosols over the Houston area may also enhance the thunderstorm intensity and precipitation

526 through the same mechanism by secondary nucleation of numerous ultrafine aerosol particles from

527 the anthropogenic sources. But the magnitude of the effect is not as substantial as in the Amazon

528 environment. Possible reasons include that background aerosols are much higher over the Houston

529 area and air is not as humid as Amazon.

Acknowledgments

540

Reference

Abdul-Razzak, H., and Ghan, S. J.: A parameterization of aerosol activation - 3. Sectional representation, J Geophys Res-Atmos, 107, 4026, doi: 10.1029/2001jd000483, 2002.

Andreae, M. O., Jones, C. D., and Cox, P. M.: Strong present-day aerosol cooling implies a hot future, Nature, 435, 1187-1190, doi: 10.1038/nature03671, 2005.

Arakawa, A.: The cumulus parameterization problem: Past, present, and future, J Climate, 17, 2493-2525, doi: 10.1175/1520-0442(2004)017<2493:Ratcpp>2.0.Co;2, 2004.

Chen, F., and Dudhia, J.: Coupling an advanced land surface-hydrology model with the Penn State-NCAR MM5 modeling system. Part I: Model implementation and sensitivity, Mon Weather Rev, 129, 569-585, doi: 10.1175/1520-0493(2001)129<0569:Caalsh>2.0.Co;2, 2001.

Chen Q., J. Fan, Y. Yin, and B. Han: Aerosol impacts on mesoscale convective systems forming under different vertical wind shear conditions. Journal of Geophysical Research: Atmospheres, 125, e2018JD030027, 2020.

Chen, Y. C., Xue, L., Lebo, Z. J., Wang, H., Rasmussen, R. M., and Seinfeld, J. H.: A comprehensive numerical study of aerosol-cloud-precipitation interactions in marine stratocumulus, Atmos Chem Phys, 11, 9749-9769, doi: 10.5194/acp-11-9749-2011, 2011.

Dagan, G., Koren, I., Altaratz, O. and Lehahn, Y.: Shallow convective cloud field lifetime as a key factor for evaluating aerosol effects. iScience, 10, 192–202, 2018.

Ekman, A. M. L., Engstrom, A., and Soderberg, A.: Impact of Two-Way Aerosol-Cloud Interaction and Changes in Aerosol Size Distribution on Simulated Aerosol-Induced Deep Convective Cloud Sensitivity, J Atmos Sci, 68, 685-698, doi: 10.1175/2010jas3651.1, 2011.

564   Fan, J. W., Zhang, R. Y., Li, G. H., and Tao, W. K.: Effects of aerosols and relative humidity on

565   cumulus clouds, J Geophys Res-Atmos, 112, D14204, doi: 10.1029/2006jd008136, 2007.

566   Fan, J. W., Yuan, T. L., Comstock, J. M., Ghan, S., Khain, A., Leung, L. R., Li, Z. Q., Martins, V.

567   J., and Ovchinnikov, M.: Dominant role by vertical wind shear in regulating aerosol effects

568   on deep convective clouds, J Geophys Res-Atmos, 114, D22206, doi:

569   10.1029/2009jd012352, 2009.

570   Fan, J. W., Leung, L. R., Li, Z. Q., Morrison, H., Chen, H. B., Zhou, Y. Q., Qian, Y., and Wang,

571   Y.: Aerosol impacts on clouds and precipitation in eastern China: Results from bin and

572   bulk microphysics, J Geophys Res-Atmos, 117, D00k36, doi: 10.1029/2011jd016537,

573   2012a.

574   Fan, J. W., Rosenfeld, D., Ding, Y. N., Leung, L. R., and Li, Z. Q.: Potential aerosol indirect effects

575   on atmospheric circulation and radiative forcing through deep convection, Geophys Res

576   Lett, 39, L09806, doi: 10.1029/2012gl051851, 2012b.

577   Fan, J. W., Leung, L. R., Rosenfeld, D., Chen, Q., Li, Z. Q., Zhang, J. Q., and Yan, H. R.:

578   Microphysical effects determine macrophysical response for aerosol impacts on deep

579   convective clouds, P Natl Acad Sci USA, 110, E4581-E4590, doi:

580   10.1073/pnas.1316830110, 2013.

581   Fan, J. W., Wang, Y., Rosenfeld, D., and Liu, X. H.: Review of Aerosol-Cloud Interactions:

582   Mechanisms, Significance, and Challenges, J Atmos Sci, 73, 4221-4252, doi: 10.1175/Jas-

583   D-16-0037.1, 2016.

584   Fan, J. W., Han, B., Varble, A., Morrison, H., North, K., Kollias, P., Chen, B. J., Dong, X. Q.,

585   Giangrande, S. E., Khain, A., Lin, Y., Mansell, E., Milbrandt, J. A., Stenz, R., Thompson,

586   G., and Wang, Y.: Cloud-resolving model intercomparison of an MC3E squall line case:

587   Part I-Convective updrafts, J Geophys Res-Atmos, 122, 9351-9378, doi:

588   10.1002/2017jd026622, 2017.

589 Fan, J. W., Rosenfeld, D., Zhang, Y. W., Giangrande, S. E., Li, Z. Q., Machado, L. A. T., Martin,

590   S. T., Yang, Y., Wang, J., Artaxo, P., Barbosa, H. M. J., Braga, R. C., Comstock, J. M.,

591   Feng, Z., Gao, W. H., Gomes, H. B., Mei, F., Pohlker, C., Pohlker, M. L., Poschl, U., and

592   de Souza, R. A. F.: Substantial convection and precipitation enhancements by ultrafine

593   aerosol particles, Science, 359, 411-418, doi: 10.1126/science.aan8461, 2018.

594 Fast, J. D., Gustafson, W. I., Easter, R. C., Zaveri, R. A., Barnard, J. C., Chapman, E. G., Grell, G.

595   A., and Peckham, S. E.: Evolution of ozone, particulates, and aerosol direct radiative

596   forcing in the vicinity of Houston using a fully coupled meteorology-chemistry-aerosol

597   model, J Geophys Res-Atmos, 111, D21305, doi: 10.1029/2005jd006721, 2006.

598 Gao, W. H., Fan, J. W., Easter, R. C., Yang, Q., Zhao, C., and Ghan, S. J.: Coupling spectral-bin

599   cloud microphysics with the MOSAIC aerosol model in WRF-Chem: Methodology and

600   results for marine stratocumulus clouds, J Adv Model Earth Sy, 8, 1289-1309, doi:

601   10.1002/2016ms000676, 2016.

602 Gelaro, R., McCarty, W., Suarez, M. J., Todling, R., Molod, A., Takacs, L., Randles, C. A.,

603   Darmenov, A., Bosilovich, M. G., Reichle, R., Wargan, K., Coy, L., Cullather, R., Draper,

604   C., Akella, S., Buchard, V., Conaty, A., da Silva, A. M., Gu, W., Kim, G. K., Koster, R.,

605   Lucchesi, R., Merkova, D., Nielsen, J. E., Partyka, G., Pawson, S., Putman, W., Rienecker,

606   M., Schubert, S. D., Sienkiewicz, M., and Zhao, B.: The Modern-Era Retrospective

607   Analysis for Research and Applications, Version 2 (MERRA-2), J Climate, 30, 5419-5454,

608   doi: 10.1175/Jcli-D-16-0758.1, 2017.

609   Grabowski, W. W., and H.Morrison: Untangling microphysical impacts on deep convection

610   applying a novel modeling methodology. Part II: Double-moment microphysics. J. Atmos.

611   Sci., 73, 3749–3770, 2016.

612   Grabowski, W. W., and H. Morrison: Modeling condensation in deep convection, J. Atmos.

613   Sci., 74, 2247– 2267, doi:10.1175/JAS-D-16-0255.1, 2017.

614   Grabowski, W. W., and H. Morrison: Do ultrafine cloud condensation nuclei invigorate deep

615   convection? J. Atmos. Sci., 77(7), 2567-2583, doi: 10.1175/JAS-D-20-0012.1, 2020.

616   Grell, G. A., Peckham, S. E., Schmitz, R., McKeen, S. A., Frost, G., Skamarock, W. C., and Eder,

617   B.: Fully coupled "online" chemistry within the WRF model, Atmos Environ, 39, 6957-

618   6975, doi: 10.1016/j.atmosenv.2005.04.027, 2005.

619   Guenther, A., Karl, T., Harley, P., Wiedinmyer, C., Palmer, P. I., and Geron, C.: Estimates of

620   global terrestrial isoprene emissions using MEGAN (Model of Emissions of Gases and

621   Aerosols from Nature), Atmos Chem Phys, 6, 3181-3210, doi: 10.5194/acp-6-3181-2006,

622   2006.

623   Haywood, J., and Boucher, O.: Estimates of the direct and indirect radiative forcing due to

624   tropospheric aerosols: A review, Rev Geophys, 38, 513-543, doi: 10.1029/1999rg000078,

625   2000.

626   Houze, R. A.: Cloud dynamics, 2. edn., Elsevier/Acad. Press, Amsterdam, 2014.

627   Iacono, M. J., Delamere, J. S., Mlawer, E. J., Shephard, M. W., Clough, S. A., and Collins, W. D.:

628   Radiative forcing by long-lived greenhouse gases: Calculations with the AER radiative

629   transfer models, J Geophys Res-Atmos, 113, D13103, doi: 10.1029/2008jd009944, 2008.

630   Janjic, Z. I.: The Step-Mountain Eta Coordinate Model - Further Developments of the Convection,

631   Viscous Sublayer, and Turbulence Closure Schemes, Mon Weather Rev, 122, 927-945, doi:

632   10.1175/1520-0493(1994)122<0927:Tsmecm>2.0.Co;2, 1994.

633   Khain, A., Pokrovsky, A., Pinsky, M., Seifert, A., and Phillips, V.: Simulation of effects of

634   atmospheric aerosols on deep turbulent convective clouds using a spectral microphysics

635   mixed-phase cumulus cloud model. Part I: Model description and possible applications, J

636   Atmos Sci, 61, 2963-2982, doi: 10.1175/Jas-3350.1, 2004.

637   Khain, A., Rosenfeld, D., and Pokrovsky, A.: Aerosol impact on the dynamics and microphysics

638   of deep convective clouds, Q J Roy Meteor Soc, 131, 2639-2663, doi: 10.1256/qj.04.62,

639   2005.

640   Khain, A., and Lynn, B.: Simulation of a supercell storm in clean and dirty atmosphere using

641   weather research and forecast model with spectral bin microphysics, J Geophys Res-Atmos,

642   114, D19209, doi: 10.1029/2009jd011827, 2009.

643   Khain, A., Lynn, B., and Dudhia, J.: Aerosol Effects on Intensity of Landfalling Hurricanes as

644   Seen from Simulations with the WRF Model with Spectral Bin Microphysics, J Atmos Sci,

645   67, 365-384, doi: 10.1175/2009jas3210.1, 2010.

646   Khain, A. P., BenMoshe, N., and Pokrovsky, A.: Factors determining the impact of aerosols on

647   surface precipitation from clouds: An attempt at classification, J Atmos Sci, 65, 1721-1748,

648   doi: 10.1175/2007jas2515.1, 2008.

649   Khain, A. P., Leung, L. R., Lynn, B., and Ghan, S.: Effects of aerosols on the dynamics and

650   microphysics of squall lines simulated by spectral bin and bulk parameterization schemes,

651   J Geophys Res-Atmos, 114, D22203, doi: 10.1029/2009jd011902, 2009.

652 Khain, A. P., Beheng, K. D., Heymsfield, A., Korolev, A., Krichak, S. O., Levin, Z., Pinsky, M.,

653   Phillips, V., Prabhakaran, T., Teller, A., van den Heever, S. C., and Yano, J. I.:

654   Representation of microphysical processes in cloud-resolving models: Spectral (bin)

655   microphysics versus bulk parameterization, Rev Geophys, 53, 247-322, doi:

656   10.1002/2014rg000468, 2015.

657 Koren, I., Dagan, G., and Altaratz, O.: From aerosol-limited to invigoration of warm convective

658   clouds, Science, 344, 1143-1146, doi: 10.1126/science.1252595, 2014.

659 Korolev A., and I. Mazin: Supersaturation of water vapor in clouds. J. Atmos. Sci., 60, 2957-2974,

660   2003.

661 Lebo, Z.: A Numerical Investigation of the Potential Effects of Aerosol-Induced Warming and

662   Updraft Width and Slope on Updraft Intensity in Deep Convective Clouds, J Atmos Sci,

663   75, 535-554, doi: 10.1175/Jas-D-16-0368.1, 2018.

664 Lebo, Z. J., and Seinfeld, J. H.: Theoretical basis for convective invigoration due to increased

665   aerosol concentration, Atmos Chem Phys, 11, 5407-5429, doi: 10.5194/acp-11-5407-2011,

666   2011.

667 Lebo, Z. J., Morrison, H., and Seinfeld, J. H.: Are simulated aerosol-induced effects on deep

668   convective clouds strongly dependent on saturation adjustment? Atmos Chem Phys, 12,

669   9941-9964, doi: 10.5194/acp-12-9941-2012, 2012.

670 Lee, S. S., Li, Z. Q., Zhang, Y. W., Yoo, H., Kim, S., Kim, B. G., Choi, Y. S., Mok, J., Um, J.,

671   Choi, K. O., and Dong, D. H.: Effects of model resolution and parameterizations on the

672   simulations of clouds, precipitation, and their interactions with aerosols, Atmos Chem Phys,

673   18, 13-29, doi: 10.5194/acp-18-13-2018, 2018.

674   Li, G. H., Wang, Y., and Zhang, R. Y.: Implementation of a two-moment bulk microphysics

675   scheme to the WRF model to investigate aerosol-cloud interaction, J Geophys Res-Atmos,

676   113, D15211, doi: 10.1029/2007jd009361, 2008.

677   Li, X. W., Tao, W. K., Khain, A. P., Simpson, J., and Johnson, D. E.: Sensitivity of a Cloud-

678   Resolving Model to Bulk and Explicit Bin Microphysical Schemes. Part I: Comparisons, J

679   Atmos Sci, 66, 3-21, doi: 10.1175/2008jas2646.1, 2009.

680   Li, Z. Q., Niu, F., Fan, J. W., Liu, Y. G., Rosenfeld, D., and Ding, Y. N.: Long-term impacts of

681   aerosols on the vertical development of clouds and precipitation, Nat Geosci, 4, 888-894,

682   doi: 10.1038/Ngeo1313, 2011.

683   Loftus, A. M., and Cotton, W. R.: Examination of CCN impacts on hail in a simulated supercell

684   storm with triple-moment hail bulk microphysics, Atmos Res, 147, 183-204, doi:

685   10.1016/j.atmosres.2014.04.017, 2014.

686   Lohmann, U., and Feichter, J.: Global indirect aerosol effects: a review, Atmos Chem Phys, 5,

687   715-737, doi: 10.5194/acp-5-715-2005, 2005.

688   Milbrandt, J. A., and Yau, M. K.: A multimoment bulk microphysics parameterization. Part II: A

689   proposed three-moment closure and scheme description, J Atmos Sci, 62, 3065-3081, doi:

690   10.1175/Jas3535.1, 2005.

691   Morrison, H., Curry, J. A., and Khvorostyanov, V. I.: A new double-moment microphysics

692   parameterization for application in cloud and climate models. Part I: Description, J Atmos

693   Sci, 62, 1665-1677, doi: 10.1175/Jas3446.1, 2005.

694   Morrison, H., and W. W.Grabowski: Comparison of bulk and bin warm-rain microphysics models

695   using a kinematic framework.J. Atmos. Sci., 64, 2839–2861, 2007.

696   Morrison, H., and W. W. Grabowski: Modeling supersaturation and subgrid-scale mixing with

697   two-moment bulk warm microphysics, J. Atmos. Sci., 65, 792–812,

698   doi:10.1175/2007JAS2374.1, 2008.

699   Morrison, H., Thompson, G., and Tatarskii, V.: Impact of Cloud Microphysics on the Development

700   of Trailing Stratiform Precipitation in a Simulated Squall Line: Comparison of One- and

701   Two-Moment Schemes, Mon Weather Rev, 137, 991-1007, doi: 10.1175/2008mwr2556.1,

702   2009.

703   Morrison, H., and Milbrandt, J.: Comparison of Two-Moment Bulk Microphysics Schemes in

704   Idealized Supercell Thunderstorm Simulations, Mon Weather Rev, 139, 1103-1130, doi:

705   10.1175/2010mwr3433.1, 2011.

706   Morrison, H.: On the robustness of aerosol effects on an idealized supercell storm simulated with

707   a cloud system-resolving model, Atmos Chem Phys, 12, 7689-7705, doi: 10.5194/acp-12-

708   7689-2012, 2012.

709   Pinsky M., I.P. Mazin, A. Korolev, and A.P. Khain: Supersaturation and diffusional droplet growth

710   in liquid clouds. J. Atmos. Sci. 70, 2778-2793, 2013.

711   Politovich, M. K., and W. A. Cooper: Variability of the supersaturation in cumulus clouds. J.

712   Atmos. Sci., 45, 1651–1664, doi:10.1175/1520-0469(1988)045,1651:VOTSIC.2.0.CO;2,

713   1988.

714   Rosenfeld, D., Lohmann, U., Raga, G. B., O'Dowd, C. D., Kulmala, M., Fuzzi, S., Reissell, A.,

715   and Andreae, M. O.: Flood or drought: How do aerosols affect precipitation?, Science, 321,

716   1309-1313, doi: 10.1126/science.1160606, 2008.

717   Rosenfeld, D., Andreae, M. O., Asmi, A., Chin, M., de Leeuw, G., Donovan, D. P., Kahn, R.,

718   Kinne, S., Kivekas, N., Kulmala, M., Lau, W., Schmidt, K. S., Suni, T., Wagner, T., Wild,

719   M., and Quaas, J.: Global observations of aerosol-cloud-precipitation-climate interactions,

720   Rev Geophys, 52, 750-808, doi: 10.1002/2013rg000441, 2014.

721   Rosenfeld, D., Zheng, Y. T., Hashimshoni, E., Pohlker, M. L., Jefferson, A., Pohlker, C., Yu, X.,

722   Zhu, Y. N., Liu, G. H., Yue, Z. G., Fischman, B., Li, Z. Q., Giguzin, D., Goren, T., Artaxo,

723   P., Barbosa, H. M. J., Poschl, U., and Andreae, M. O.: Satellite retrieval of cloud

724   condensation nuclei concentrations by using clouds as CCN chambers, P Natl Acad Sci

725   USA, 113, 5828-5834, doi: 10.1073/pnas.1514044113, 2016.

726   Salamanca, F., and Martilli, A.: A new Building Energy Model coupled with an Urban Canopy

727   Parameterization for urban climate simulations-part II. Validation with one dimension off-

728   line simulations, Theor Appl Climatol, 99, 345-356, doi: 10.1007/s00704-009-0143-8,

729   2010.

730   Sheffield, A. M., Saleeby, S. M., and van den Heever, S. C.: Aerosol-induced mechanisms for

731   cumulus congestus growth, J Geophys Res-Atmos, 120, 8941-8952, doi:

732   10.1002/2015jd023743, 2015.

733   Skamarock, W. C., Klemp, J. B., Dudhia, J., Gill, D. O., Barker, D. M., Duda, M., Huang, X. Y.,

734   Wang, W., and Powers, J. G.: A description of the advanced research WRF version 3,

735   NCAR, Tech. Note, Mesoscale and Microscale Meteorology Division, National Center for

736   Atmospheric Research, Boulder, Colorado, USA, 2008.

737   Stevens, B., and G.Feingold: Untangling aerosol effects on clouds and precipitation in a buffered

738   system. Nature, 461, 607–613, 2009.

739   Storer, R. L., van den Heever, S. C., and Stephens, G. L.: Modeling Aerosol Impacts on Convective

740   Storms in Different Environments, J Atmos Sci, 67, 3904-3915, doi:

741   10.1175/2010jas3363.1, 2010.

742 Tao, W., and X. Li: The relationship between latent heating, vertical velocity, and precipitation

743   processes: The impact of aerosols on precipitation in organized deep convective systems,

744   J. Geophys. Res. Atmos., 121(11), 6299-6320, 2016.

745 Varble A.: Erroneous attribution of deep convective invigoration to aerosol concentration. J Atmos

746   Sci, 75(4):1351–68, 2018.

747 van den Heever, S. C., G. L.Stephens, and N. B.Wood: Aerosol indirect effects on tropical

748   convection characteristics under conditions of radiative-convective equilibrium. J. Atmos.

749   Sci., 68, 699–718, 2011.

750 Wang, Y., Fan, J. W., Zhang, R. Y., Leung, L. R., and Franklin, C.: Improving bulk microphysics

751   parameterizations in simulations of aerosol effects, J Geophys Res-Atmos, 118, 5361-5379,

752   doi: 10.1002/jgrd.50432, 2013.

753 Wiedinmyer, C., Akagi, S. K., Yokelson, R. J., Emmons, L. K., Al-Saadi, J. A., Orlando, J. J., and

754   Soja, A. J.: The Fire INventory from NCAR (FINN): a high resolution global model to

755   estimate the emissions from open burning, Geosci Model Dev, 4, 625-641, doi:

756   10.5194/gmd-4-625-2011, 2011.

757 Yuan, T. L., Li, Z. Q., Zhang, R. Y., and Fan, J. W.: Increase of cloud droplet size with aerosol

758   optical depth: An observation and modeling study, J Geophys Res-Atmos, 113, D04201,

759   doi: 10.1029/2007jd008632, 2008.

760 Zaveri, R. A., Easter, R. C., Fast, J. D., and Peters, L. K.: Model for Simulating Aerosol

761   Interactions and Chemistry (MOSAIC), J Geophys Res-Atmos, 113, D13204, doi:

762   10.1029/2007jd008782, 2008.

763

764   **Table 1** Descriptions of the PM2.5 Monitoring Sites over the Houston area from TCEQ

Abbreviation	Site Descriptions	Latitude	Longitude
HA	Houston Aldine	29.901	-95.326
HDP	Houston Deer Park 2	29.670	-95.129
SFP	Seabrook Friendship Park	29.583	-95.016
CR	Conroe Relocated	30.350	-95.425
KW	Kingwood	30.058	-95.190
CT	Clinton	29.734	-95.258
PP	Park Place	29.686	-95.294
GS	Galveston 99th Street	29.254	-94.861

765

766

767

52.6
45.8
39.0
32.2
25.4
18.6
11.9
5.1

2013-06-19_22:17:54

768
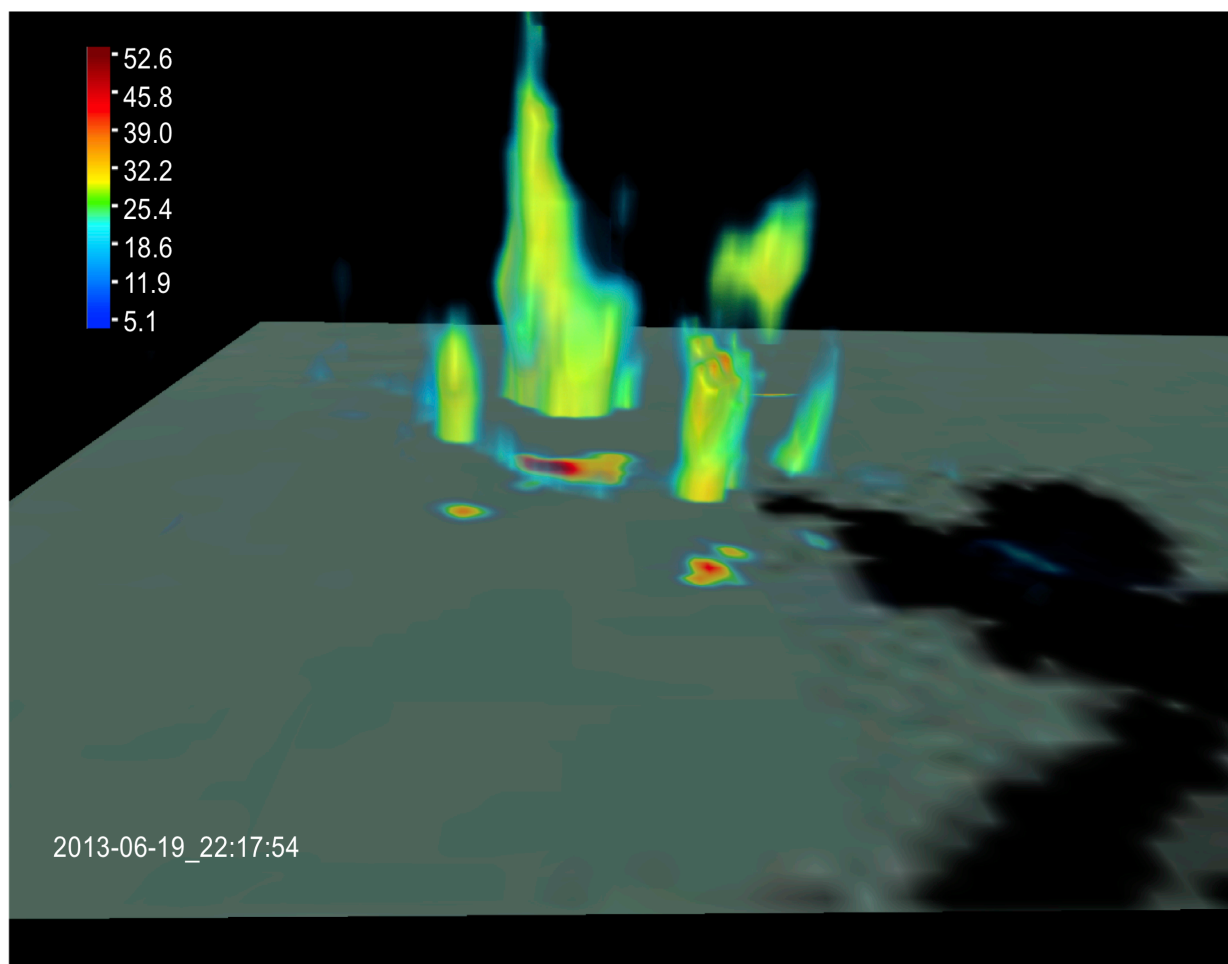
769 **Figure 1** 3D structure snapshot of radar reflectivity (unit: dBZ) from NEXRAD, overlaid with the

770 composite reflectivity shown on the surface at the time when the maximum reflectivity is observed

771 (2217 UTC). The dark shade shows the water body and the largest cell is in Houston.

772
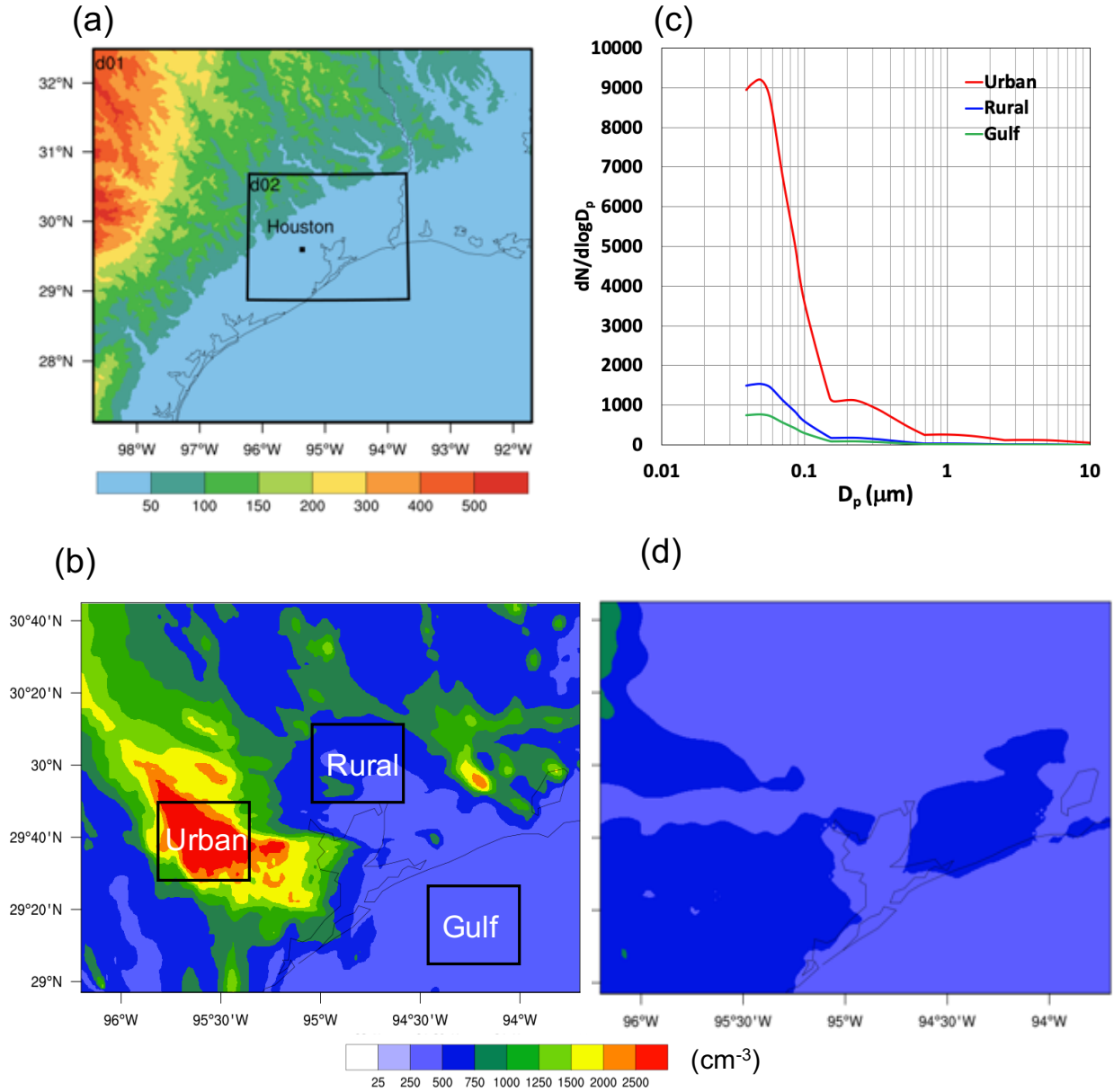
Figure 2 (a) Simulation domains with the terrain heights (unit: m), (b) aerosol number concentration (unit: cm^{-3}) from D1_MOR_anth, (c) aerosol size distributions over the urban, rural, and Gulf of Mexico as marked by three black boxes in Fig. 2b at 1200 UTC, 19 Jun 2013 (6-hr before the convection initiation), and (d) the same as Fig. 2b, but for D1_MOR_noanth in which the anthropogenic aerosols are excluded.
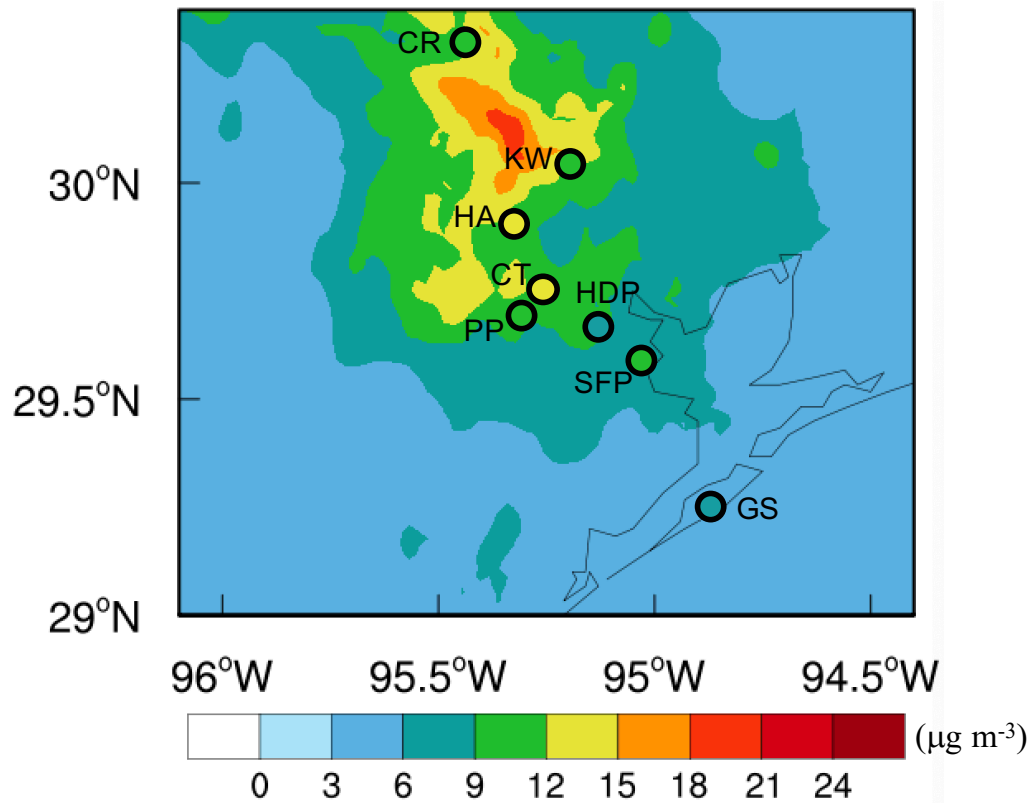
Figure 3 Comparisons of 24-hr averaged PM2.5 mass concentrations (unit: μg m^{-3}) between model simulation D1_MOR_anth (contoured) and site observation from TCEQ (colored circles) from 1800 UTC, 18 June 2013 to 1800 UTC, 19 June 2013 (1 day before the convection initiation). The site names and other information are shown in Table 1.

786
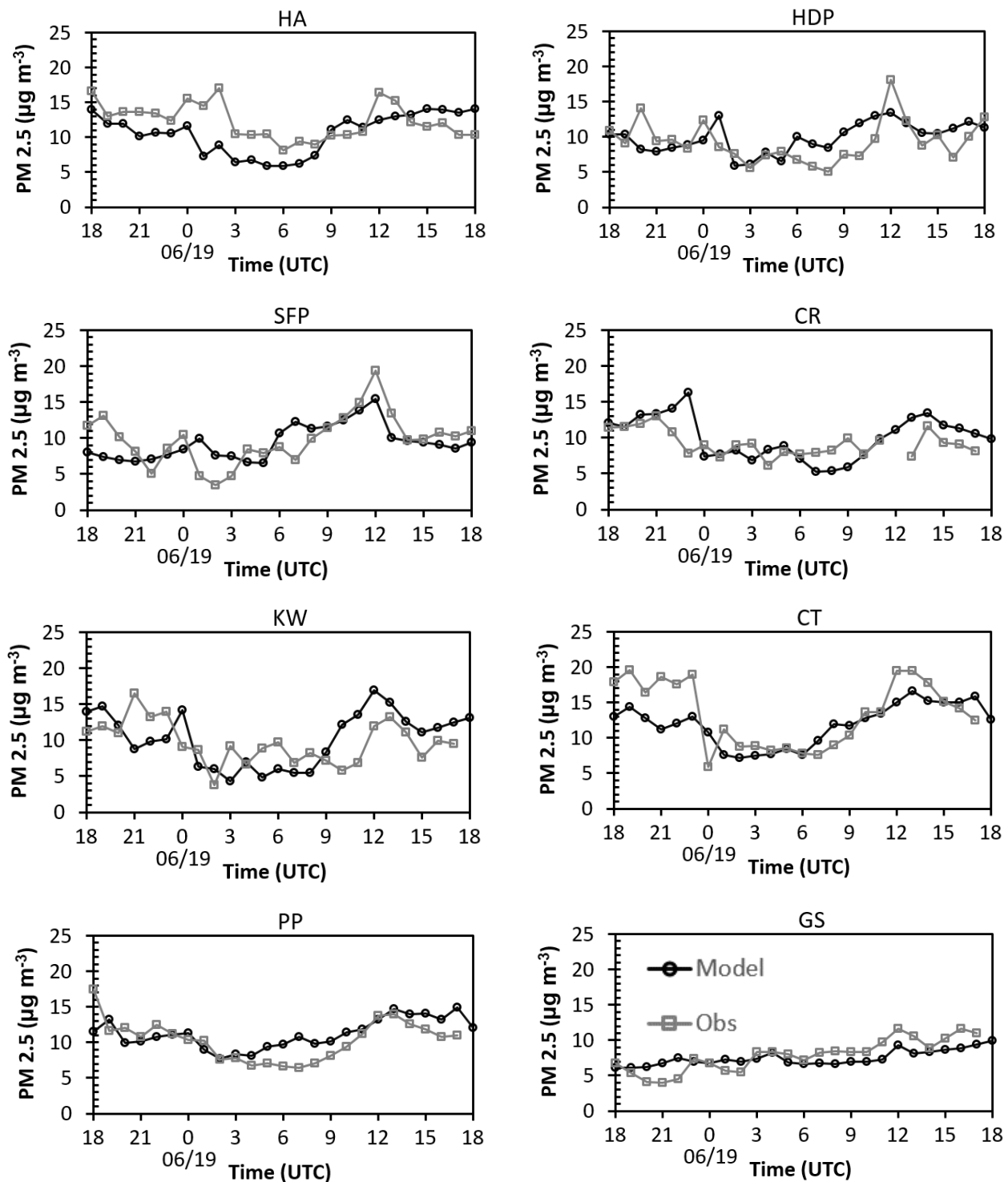
Figure 4 Site-by-site comparisons of hourly PM2.5 mass concentrations (unit: μg m^{-3}) from
D1_MOR_anth and TCEQ site observation over 24 hours from 1800 UTC, 18 June 2013 to 1800
UTC, 19 June 2013 (1 day before the convection initiation).
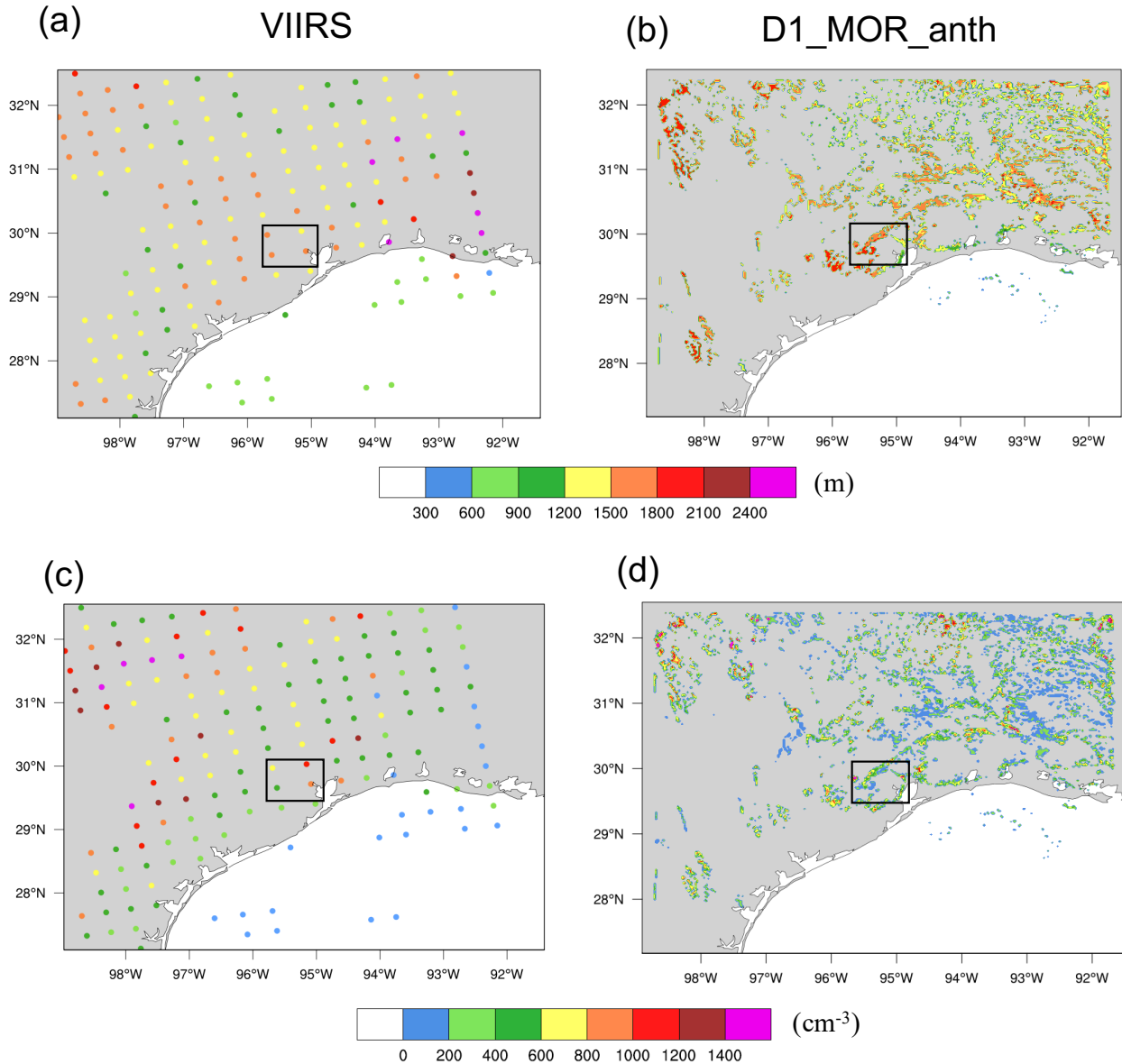
Figure 5 Evaluation of (a,b) cloud base heights (unit: m) and (c,d) CCN number concentration at cloud base (unit: cm^{-3}) from VIIRS satellite (left) retrieved at 1943 UTC (Rosenfeld et al. 2016) and model simulation D1_MOR_anth (right) at 2000 UTC, 19 June 2013. The Houston area is marked as the black box. Satellite-retrieved cloud base height was calculated from the difference between reanalysis surface air temperature (from reanalysis data) and VIIRS-measured cloud base temperature (warmest cloudy pixel) divided by the dry adiabatic lapse rate, while modeled cloud base height was determined by the lowest cloud layer with cloud mass mixing ratio greater than 10^{-5} kg kg^{-1}.
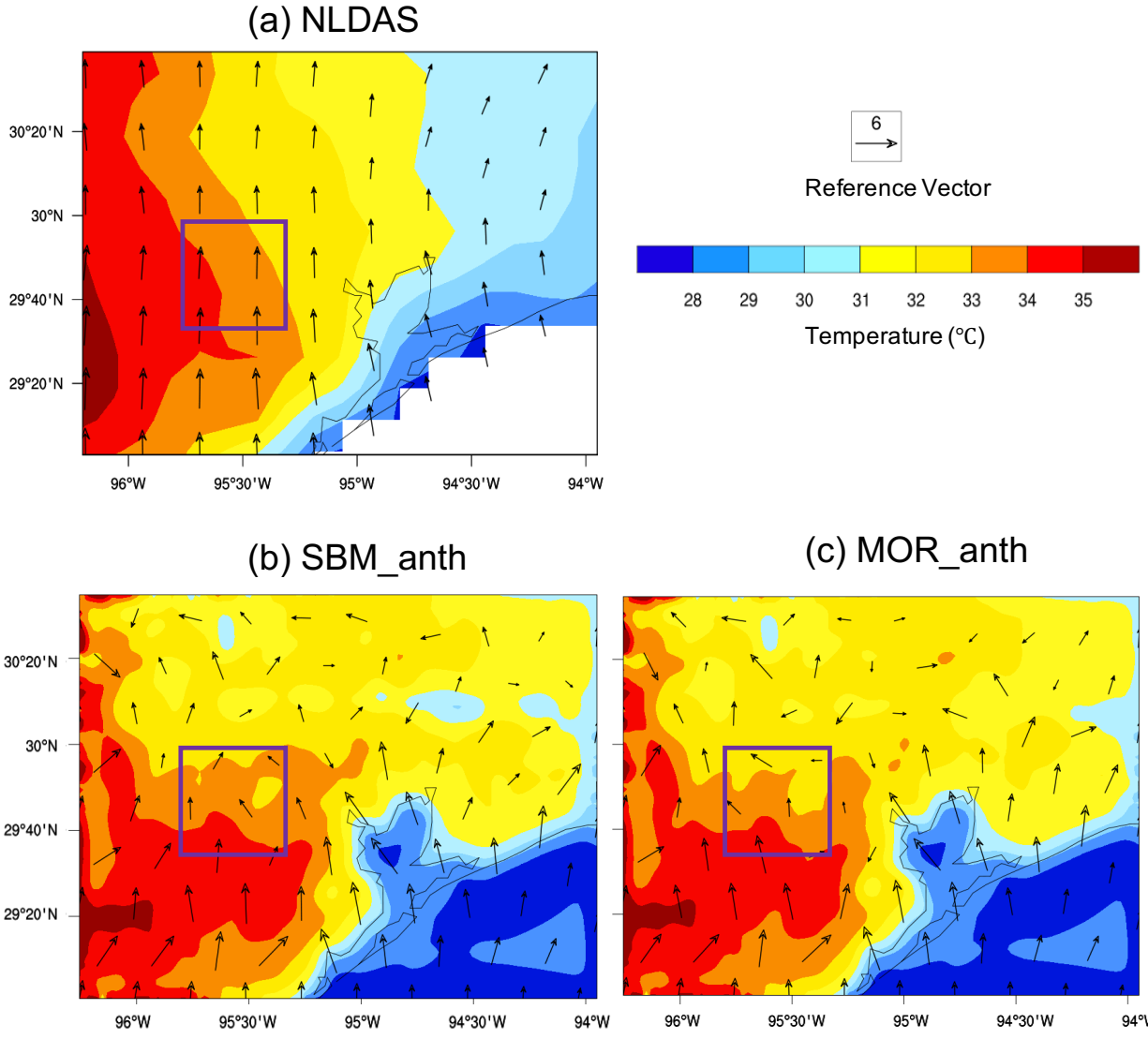
Figure 6 2-m Temperature (shaded; unit: °C) and 10-m winds (vectors; unit: m s^{-1}) from (a) NLDAS, (b) SBM_anth and (c) MOR_anth at 1800 UTC, 19 Jun 2013. The purple box denotes the Houston area.

805
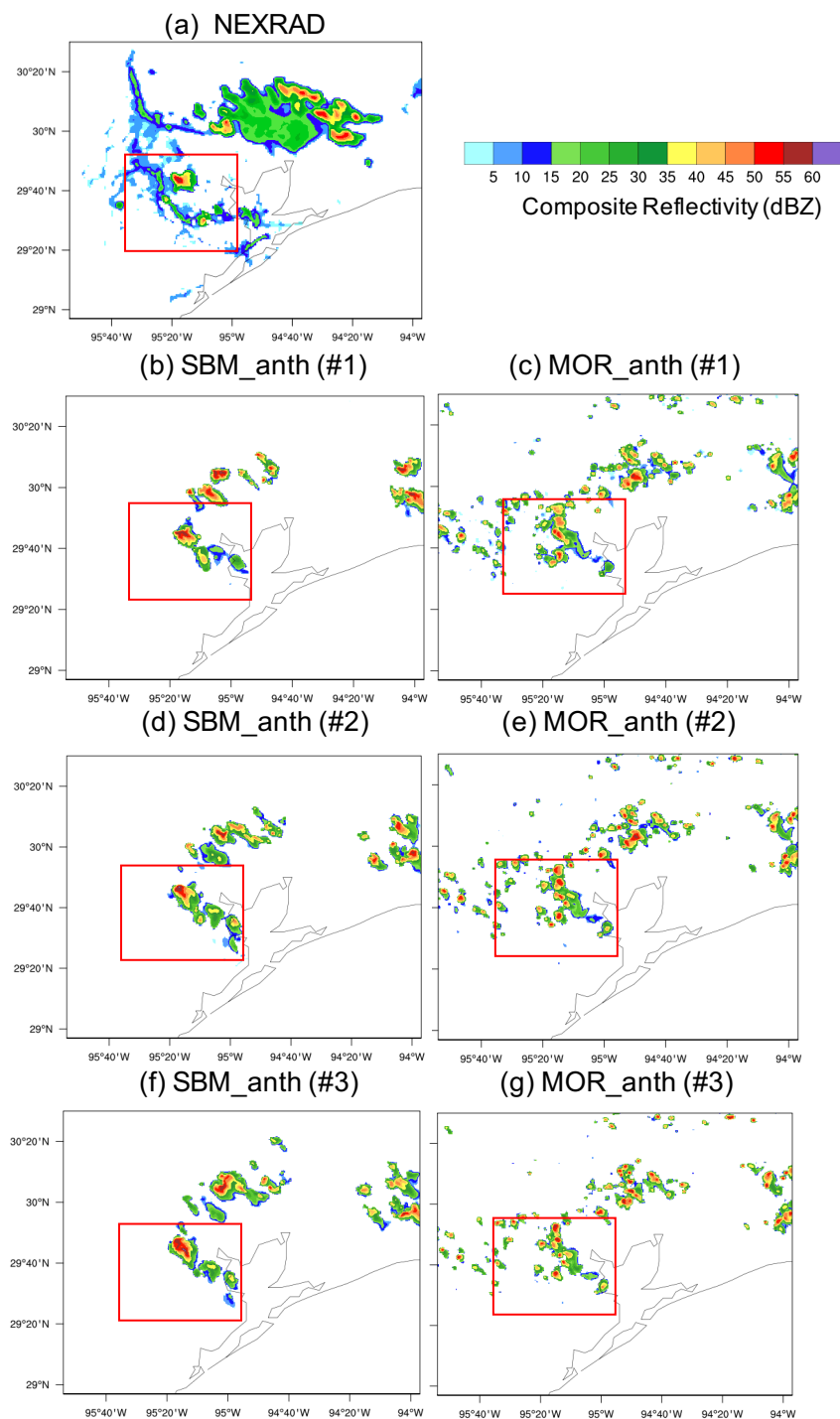
Figure 7 Composite reflectivity (unit: dBZ) from (a) NEXRAD (2217 UTC), (b, d, f) three
ensemble runs for SBM_anth (2140 UTC) and (c, e, g) three ensemble runs for MOR_anth (2125
UTC) when maximum reflectivity in Houston is observed on 19 June 2013. The red box is the
study area for convection cells near Houston.

810

(a) NEXRAD

(b) SBM_anth

(c) MOR_anth

811
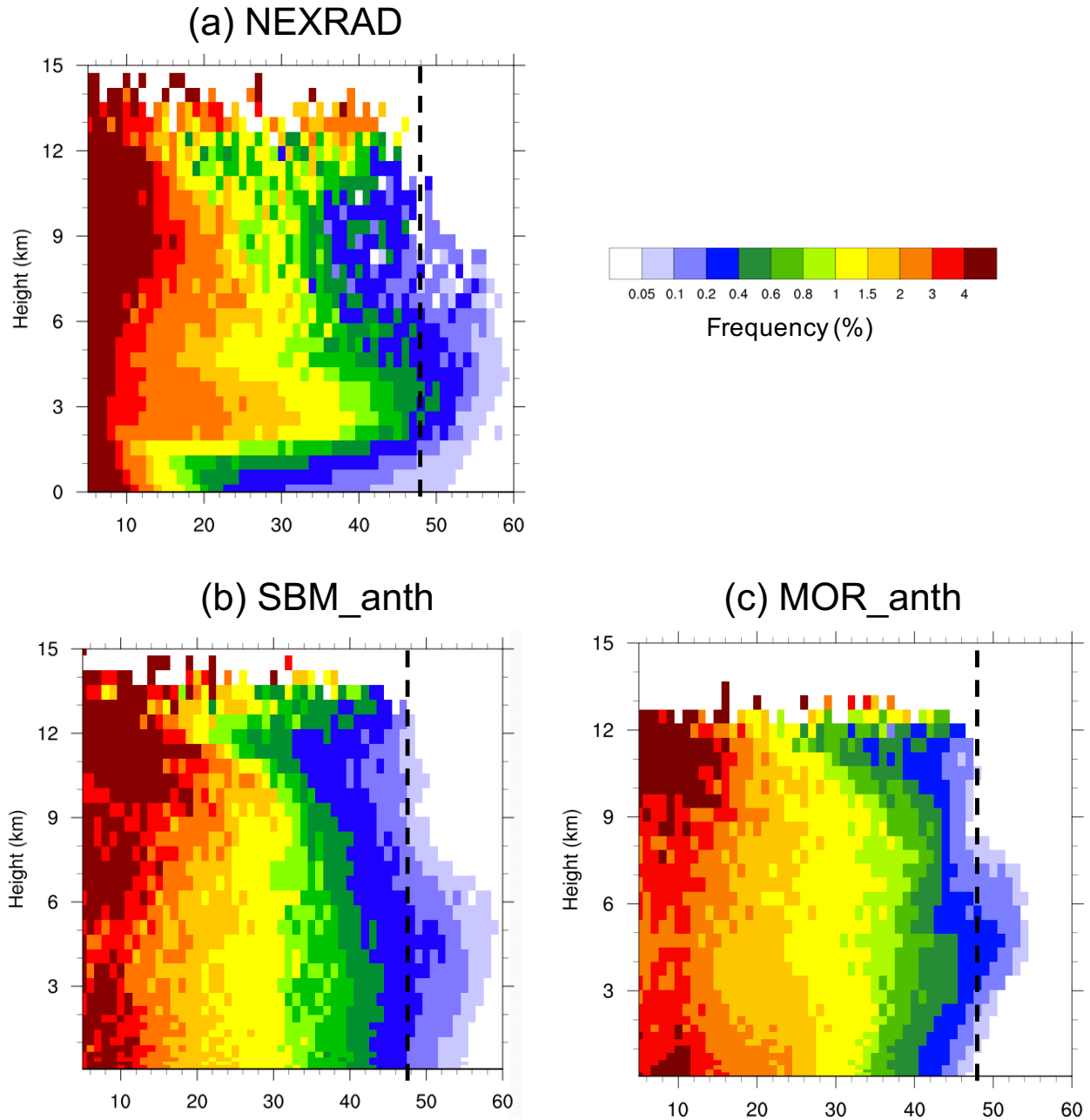
Figure 8 The CFAD of reflectivity (unit: dBZ) for the values larger than 0 dBZ from (a) NEXRAD,

(b) SBM_anth and (c) MOR_anth over the study area (red box in Fig. 7) from 1800 UTC, 19 Jun

to 0000 UTC, 20 Jun 2013. The black solid lines denote the reflectivity with the value of 48 dBZ.

The results are the three ensemble means.

816

(a)

(b)
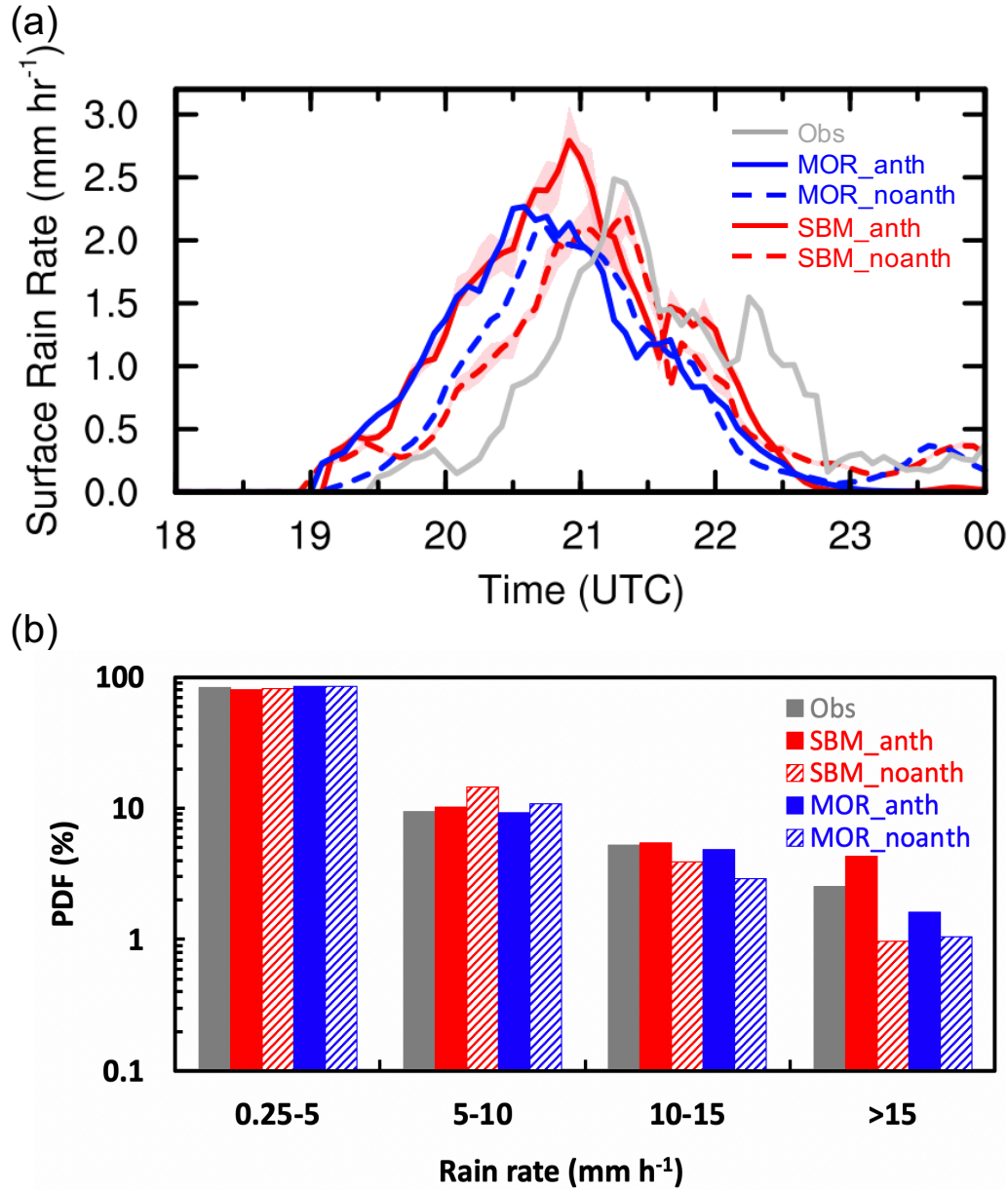
Figure 9 (a) Time series of averaged surface rain rate (unit: mm h^{-1}) and (b) PDFs of rain rate for the values larger than 0.25 mm h^{-1} over the study area (red box in Fig. 7) from observation (grey), SBM_anth and SBM_noanth (red), MOR_anth and MOR_noanth (blue) from 1800UTC, 19 Jun 2013 to 0000 UTC, 20 Jun 2013. The observed precipitation rate is obtained by NEXRAD retrieved rain rate. Both observation and model data are in every 5-min frequency. The results are the three ensemble means. The shaded areas mark the spread of the ensemble members.

(a) SBM_noanth

(b) SBM_anth

(c) MOR_noanth

(d) MOR_anth

Frequency (%)

827
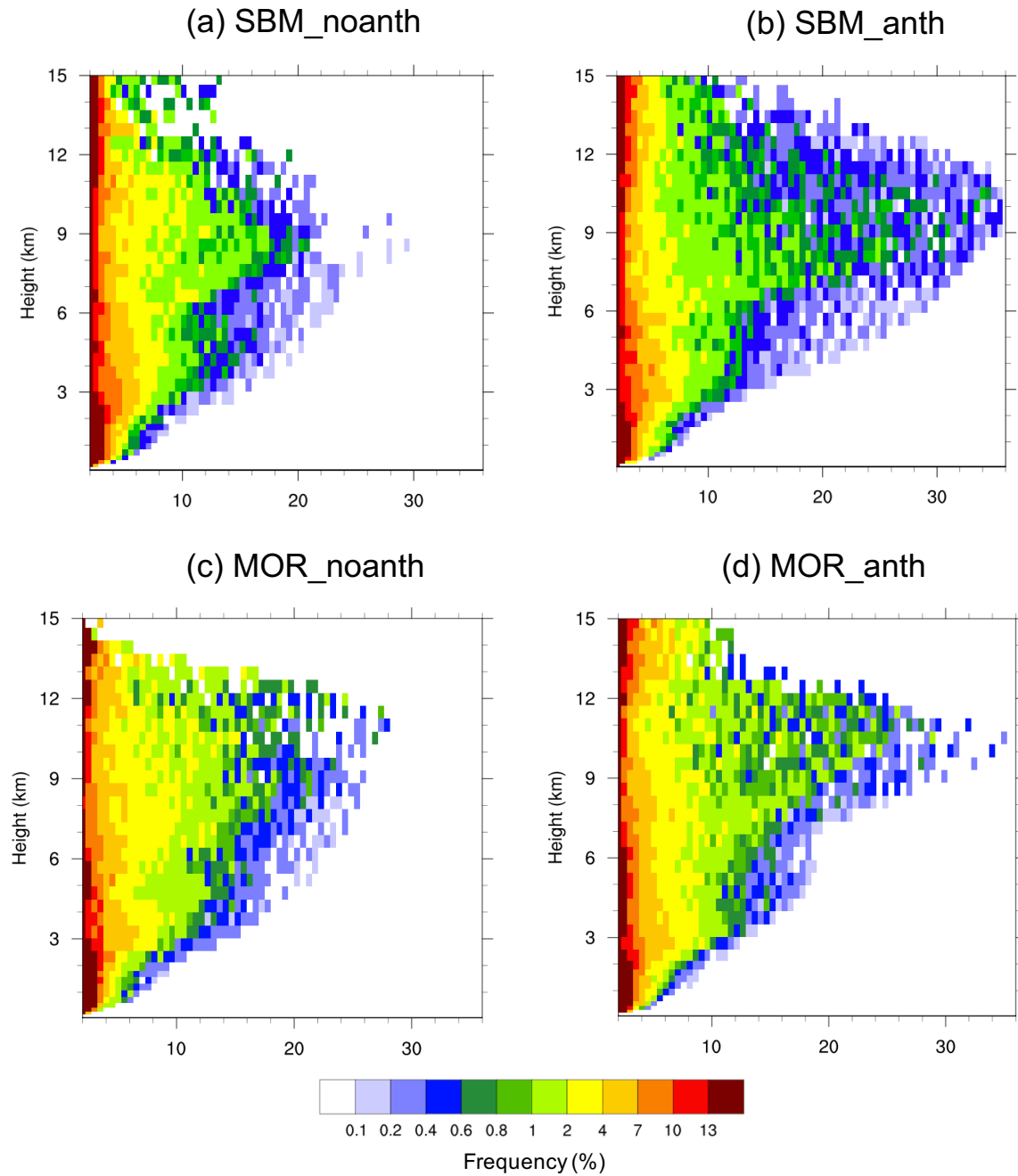
Figure 10 CFADs of updraft velocity (unit: m s^{-1}) for values larger than 2 m s^{-1} from (a)
SBM_noanth, (b) SBM_anth, (c) MOR_noanth, and (d) MOR_anth over the study area (red box
in Fig. 7) during the strong convection period (2000 – 2300 UTC, 19 Jun 2013). The results are
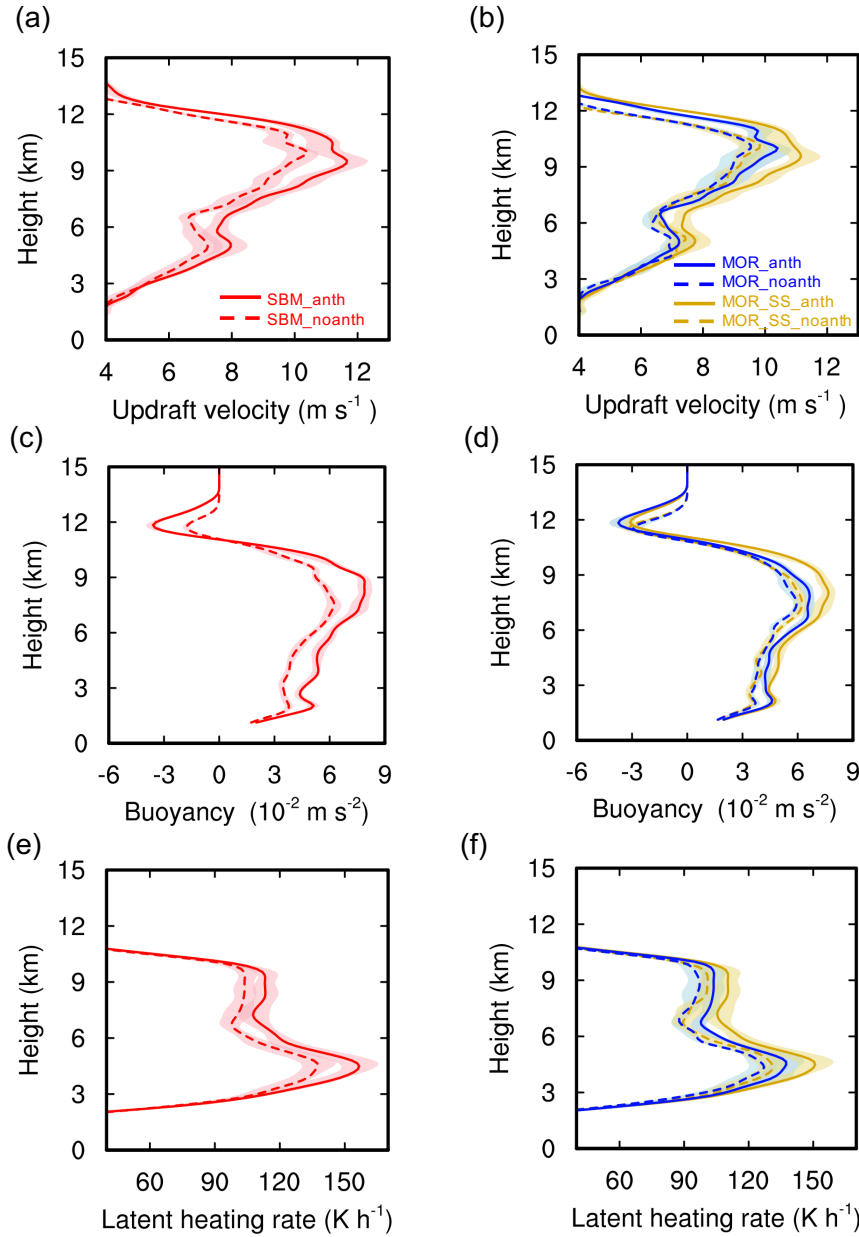the three ensemble means.

Figure 11 Vertical profiles of (a,b) updraft velocity (unit: m s^{-1}), (c,d) buoyancy (unit: m s^{-2}), and (e,f) total latent heating rate (unit: K h^{-1}) averaged over the top 25 percentiles (i.e., from 75th to 100th) of the updrafts with velocity greater than 2 m s^{-1} from the simulations SBM_anth and SBM_noanth (red), MOR_anth and MOR_noanth (blue), and MOR_SS_anth and MOR_SS_noanth (orange) over the study area (red box in Fig. 7) during the strong convection period (2000 – 2300 UTC, 19 Jun 2013). The results are the three ensemble means. The shaded areas mark the spread of the ensemble members.
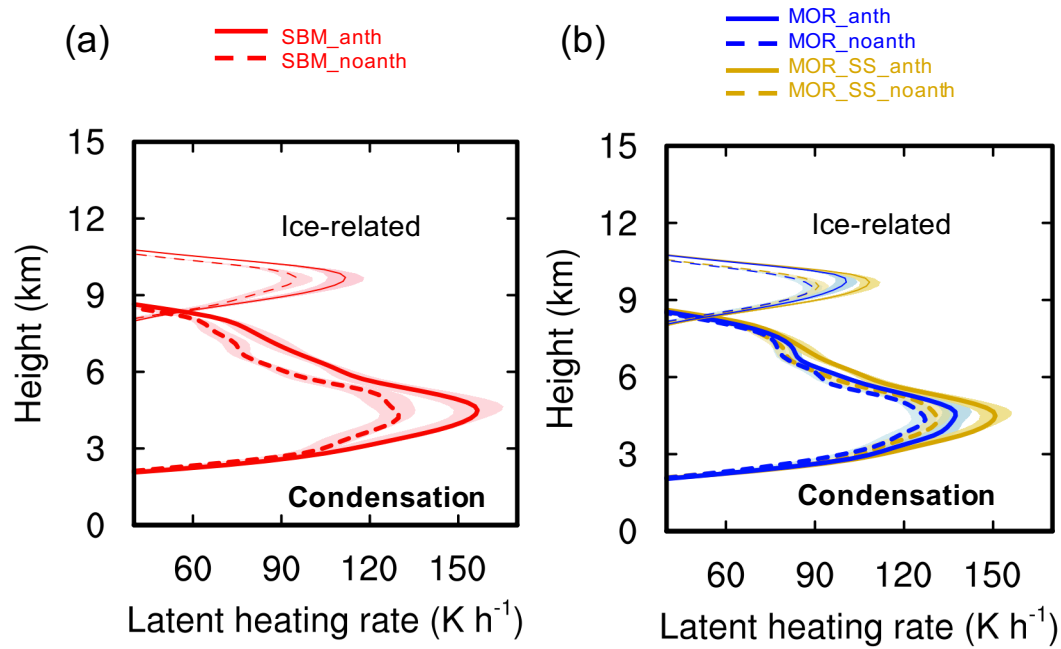
841

842 **Figure 12** Vertical profiles of condensation heating rate (thick lines below 9 km; unit: K h^{-1}) and

843 ice-related latent heating rate (thin lines above 9 km; unit: K h^{-1}) averaged over the top 25

844 percentiles (i.e., 75th to 100th) of the updrafts with a velocity greater than 2 m s^{-1} from the

845 simulations (a) SBM_anth and SBM_noanth (red), and (b) MOR_anth and MOR_noanth (blue),

846 and MOR_SS_anth and MOR_SS_noanth (orange) over the study area (red box in Fig. 7) during

847 the strong convection period (2000 – 2300 UTC, 19 Jun 2013). Data are processed in the same
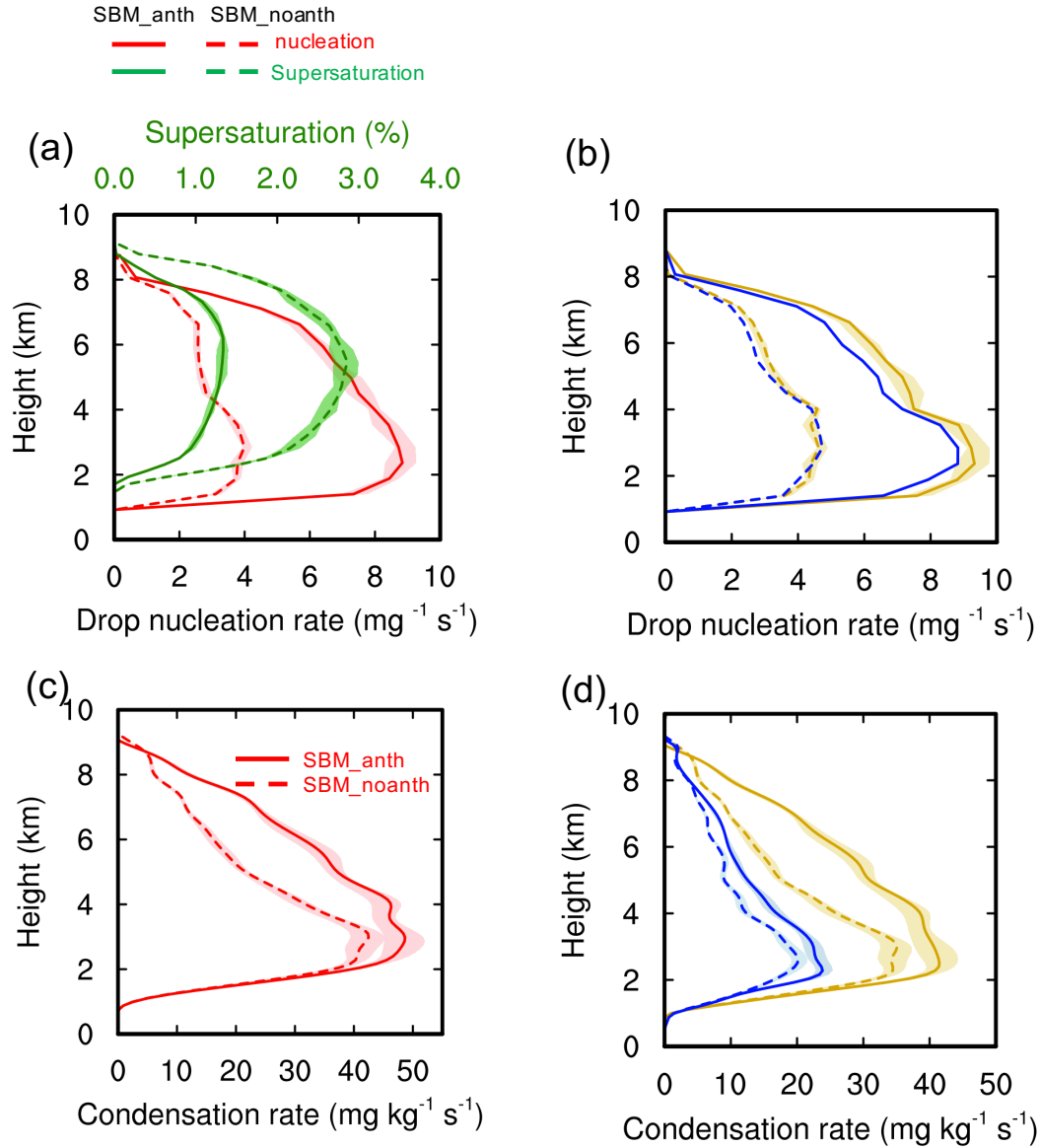
848 way as Figure 11.

849

Figure 13 Vertical profiles of (a) drop nucleation rate (red; unit: mg^{-1} s^{-1}) and supersaturation with respect to water (green; unit: %) from SBM_anth and SBM_noanth, (b) drop nucleation rate (unit: mg^{-1} s^{-1}) from MOR_anth and MOR_noanth (blue), and MOR_SS_anth and MOR_SS_noanth (orange), (c) condensation rate (unit: mg kg^{-1} s^{-1}) from SBM_anth and SBM_noanth (red), and (d) the same as (c) but from MOR_anth and MOR_noanth (blue), and MOR_SS_anth and MOR_SS_noanth (orange), averaged over the top 25 percentiles (i.e., from 75th to 100th) of the updrafts with velocity greater than 2 m s^{-1} over the study area (red box in Fig. 7) during the strong convection period (2000 – 2300 UTC, 19 Jun 2013). Data are processed in the same way as Figure 11.
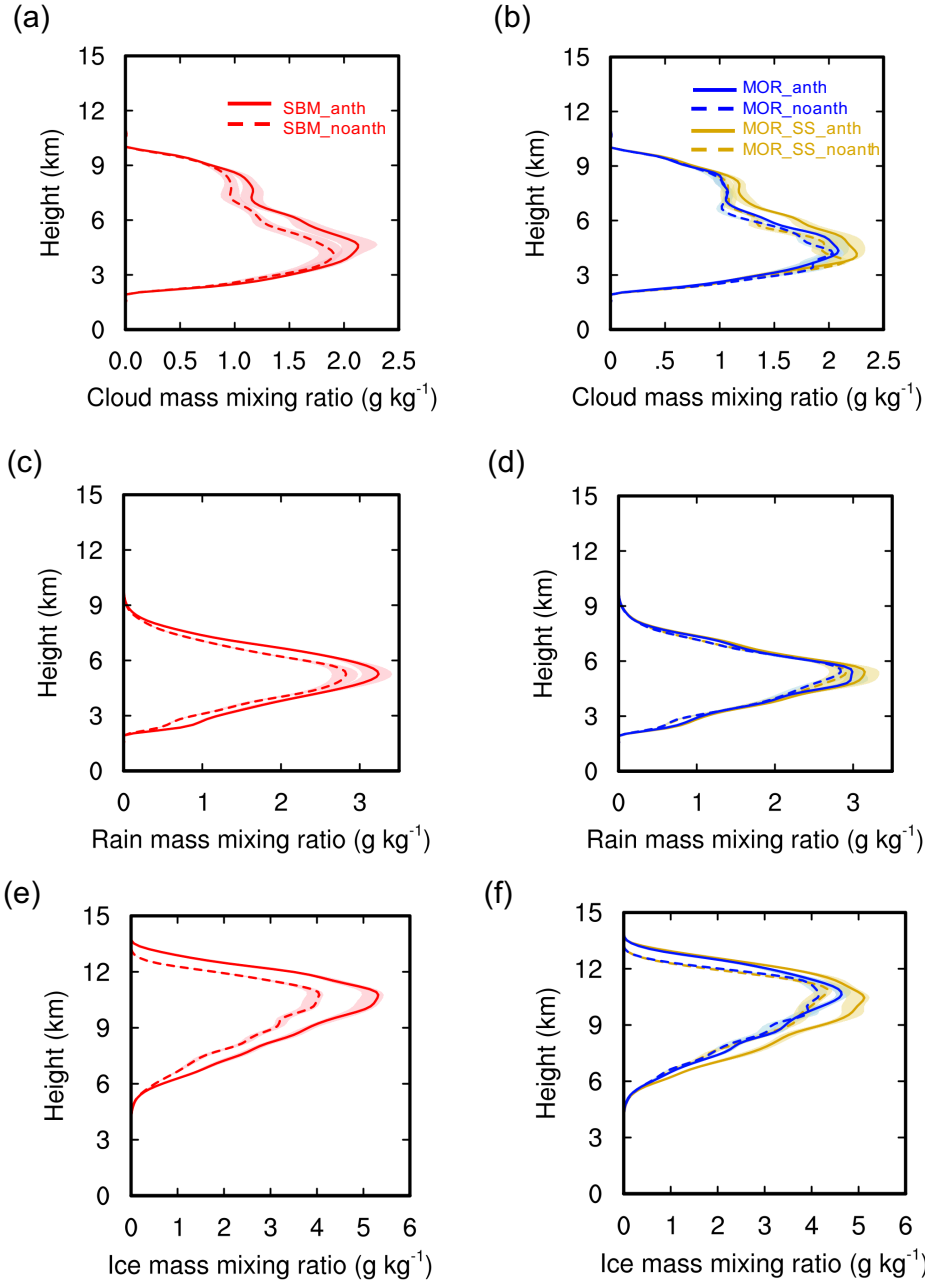
Figure 14 Vertical profiles of (a, b) cloud droplet, (c, d) raindrop and (e, f) ice particle (including ice, snow, and graupel) mass mixing ratios (unit: g kg^{-1}) averaged over the top 25 percentiles (i.e., 75th to 100th) of the updrafts with a value greater than 2 m s^{-1} from the simulations SBM_anth and SBM_noanth (red), MOR_anth and MOR_noanth (blue), and MOR_SS_anth and MOR_SS_noanth (orange) over the study area (red box in Fig. 7) during the strong convection period (2000 – 2300 UTC, 19 Jun 2013). Data are processed in the same way as Figure 11.
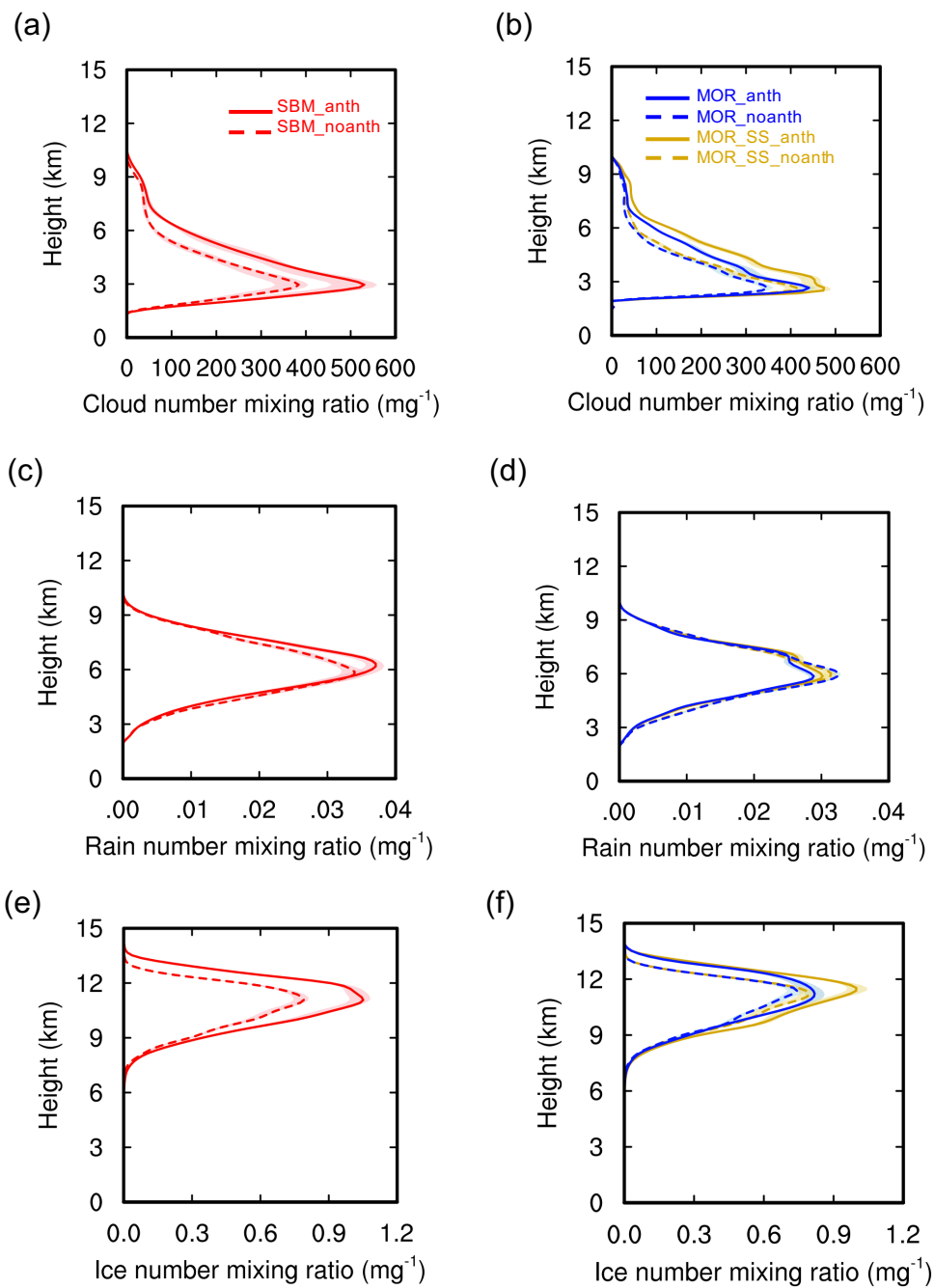
Figure 15 Same as Figure 14, but for hydrometeor number mixing ratio.

868

869

870

871